Geophysical Prospecting, 2008, **56**, 419–434 doi:10.1111/j.1365-2478.2007.00686.x

Seismic and electromagnetic controlled-source interferometry in dissipative media

Kees Wapenaar[1], Evert Slob[1] and Roel Snieder[2]

[1]*Department of Geotechnology, Delft University of Technology, PO Box 5048, 2600 GA Delft, The Netherlands, and* [2]*Center for Wave Phenomena and Department of Geophysics, Colorado School of Mines, Golden, CO 80401, USA*

Received March 2007, revision accepted November 2007

ABSTRACT

Seismic interferometry deals with the generation of new seismic responses by cross-correlating existing ones. One of the main assumptions underlying most interferometry methods is that the medium is lossless. We develop an 'interferometry-by-deconvolution' approach which circumvents this assumption. The proposed method applies not only to seismic waves, but to any type of diffusion and/or wave field in a dissipative medium. This opens the way to applying interferometry to controlled-source electromagnetic (CSEM) data. Interferometry-by-deconvolution replaces the overburden by a homogeneous half space, thereby solving the shallow sea problem for CSEM applications. We demonstrate this at the hand of numerically modeled CSEM data.

INTRODUCTION

Seismic interferometry is the branch of science that deals with the creation of new seismic responses by crosscorrelating seismic observations at different receiver locations. Since its introduction around the turn of the century, the literature on seismic interferometry has grown spectacularly. Interferometric methods have been developed for random fields (Larose *et al.* 2006; Gerstoft *et al.* 2006; Draganov *et al.* 2007) as well as for controlled-source data (Schuster and Zhou 2006; Bakulin and Calvert 2006). The underlying theories range from diffusion theory for enclosures (Weaver and Lobkis 2001), stationary phase theory (Schuster *et al.* 2004; Snieder 2004) to reciprocity theory (Wapenaar *et al.* 2004; Weaver and Lobkis 2004; van Manen *et al.* 2005). All these theories have in common the underlying assumption that the medium is lossless and non-moving. The main reason for this assumption is that the wave equation in lossless non-moving media is invariant for time-reversal, which facilitates the derivation.

Until 2005 it was commonly thought that time-reversal invariance was a necessary condition for interferometry, but recent research shows that this assumption can be relaxed. Slob, Draganov and Wapenaar (2006) analyzed the interferometric method for ground-penetrating radar data (GPR), in which losses play a prominent role. They showed that losses lead to amplitude errors as well as to the occurrence of spurious events. By choosing the recording locations in a specific way, the spurious events arrive before the first desired arrival and can thus be identified. Snieder (2006, 2007) followed a different approach. He showed that a volume distribution of uncorrelated noise sources, with source strengths proportional to the dissipation parameters of the medium, precisely compensates for the energy losses. As a consequence, the responses obtained by interferometry for this situation are free of spurious events and their amplitudes decay the way they should in a dissipative medium. This approach does not only hold for waves in dissipative media, but also for pure diffusion processes.

Time-reversal invariance as well as source-receiver reciprocity break down in flowing or rotating media, but with some minor modifications interferometry also appears to work for these situations (Wapenaar 2006; Godin 2006; Ruigrok, Draganov and Wapenaar 2008). Recently we showed that interferometry, including its extensions for waves and diffusion in dissipative and/or moving media, can be represented in a unified form (Wapenaar *et al.* 2006; Snieder, Wapenaar and Wegler 2007). In turn, from this unified formulation it follows that the interferometric method can also be used for

more exotic applications like electroseismic prospecting and quantum mechanics.

Interferometry in the strict sense makes use of crosscorrelations, but in the following we will extend the definition of interferometry so that it also includes crossconvolution and deconvolution methods. Slob, Draganov and Wapenaar (2007) introduce interferometry by crossconvolution and show that it is valid for arbitrary dissipative media. The crossconvolution method does not require a volume distribution of sources, but one restriction is that it only works for transient signals in specific configurations with receivers at opposite sides of the source array. The latter restriction does not apply to 'interferometry-by-deconvolution', which is the method discussed in this paper.

INTERFEROMETRY-BY-DECONVOLUTION: 1D VERSION

'Interferometry-by-deconvolution' is a generalization of a 1D deconvolution method introduced by Riley and Claerbout (1976). Here we briefly review this 1D method. The 3D extension is introduced in the next section.

Consider a plane wave experiment in a horizontally layered medium. At a particular depth level the total wave field is decomposed into down going and up going waves. Assuming the actual source is situated above this depth level, the total down going wave field can be seen as the illuminating wave field and the total up going wave field as its response. Subsequently, the up going wave field is deconvolved by the down going wave field. The deconvolution result is the reflection impulse response of the 1D medium below the chosen depth level. In the frequency domain, where deconvolution is replaced by division, this can be formulated as

$$\hat{R}_0^+(x_{3,1}, \omega) = \hat{p}^-(x_{3,1}, \omega)/\hat{p}^+(x_{3,1}, \omega), \tag{1}$$

where $x_{3,1}$ is the x_3-coordinate of the depth level at which the decomposition and division take place (in this paper the x_3-axis points downwards), and $\hat{p}^+$ and $\hat{p}^-$ are the down going and up going wave fields, respectively (the Fourier transform of a time-dependent function $f(t)$ is defined as $\hat{f}(\omega) = \int_{-\infty}^{\infty} f(t) \exp(-j\omega t) \mathrm{d}t$, where j is the imaginary unit and ω denotes the angular frequency, which is taken as non-negative throughout this paper). The reflection response $\hat{R}_0^+(x_{3,1}, \omega)$ is the response that would be measured with source and receiver at $x_{3,1}$ and a homogeneous half-space above $x_{3,1}$. This is independent of the actual configuration above $x_{3,1}$. For example, if $x_{3,1}$ is chosen just below the sea-bottom, $\hat{R}_0^+(x_{3,1}, \omega)$ is the response of the medium below the sea-bottom, free of multiples related to the sea-bottom as well as to the water surface. Hence, $\hat{R}_0^+(x_{3,1}, \omega)$ obeys different boundary conditions than $\hat{p}^+$ and $\hat{p}^-$.

Throughout this paper we will loosely use the term 'deconvolution' for division in the frequency domain (as in equation (1)). When the division is carried out for a sufficient range of frequencies, the result can be inverse Fourier transformed, yielding the time domain deconvolution result (e.g. $R_0^+(x_{3,1}, t)$).

The analogy of equation (1) with interferometry is as follows (see also Snieder, Sheiman and Calvert 2006): the right-hand side is a 'deconvolution' of two received wave fields (instead of a correlation of two wave fields), whereas the left-hand side is the response of a virtual source at the position of a receiver (just as in interferometry). Moreover, independent of the actual source signature (transient or noise), the time domain deconvolution result $R_0^+(x_{3,1}, t)$ is an impulse response. Of course in practice the division in equation (1) should be carried out in a stabilized sense, meaning that the result becomes a band-limited impulse response. An important difference with most versions of interferometry is that equation (1) remains valid even when the medium is dissipative. Another difference is that the application of equation (1) changes the boundary conditions, as explained above.

Bakulin and Calvert (2006) proposed a similar 1D deconvolution to improve their virtual source method. Snieder, Sheiman and Calvert (2006) employed a variant of this method (with source and receiver at different depth levels) to derive the impulse response of a building from earthquake data, and Mehta, Snieder and Graizer (2007) used a similar approach to estimate the near-surface properties of a dissipative medium.

INTERFEROMETRY-BY-DECONVOLUTION: 3D SCALAR VERSION

The 1D deconvolution approach formulated by equation (1) has been extended by various authors to a multi-dimensional deconvolution method as a means for surface related and sea-bottom related multiple elimination (Wapenaar and Verschuur 1996; Ziolkowski, Taylor and Johnston 1998; Amundsen 1999; Wapenaar *et al.* 2000; Holvik and Amundsen 2005). In the following we derive this multi-dimensional deconvolution method along the same lines as our derivation for seismic interferometry by crosscorrelation (Wapenaar, Thorbecke and Draganov 2004). First we consider the situation for scalar fields; in the next section we generalize the derivation for vector fields. Note that when we speak of 'fields' we mean wave and/or diffusion fields.

The starting point for our derivation is a reciprocity theorem of the convolution type for one-way scalar fields, which reads in the space-frequency domain

$$\int_{\partial \mathrm{D}_1} \{\hat{p}_A^+ \hat{p}_B^- - \hat{p}_A^- \hat{p}_B^+\} \mathrm{d}^2\mathbf{x} = \int_{\partial \mathrm{D}_m} \{\hat{p}_A^+ \hat{p}_B^- - \hat{p}_A^- \hat{p}_B^+\} \mathrm{d}^2\mathbf{x}, \tag{2}$$

where $\mathbf{x} = (x_1, x_2, x_3)$ is the Cartesian coordinate vector, $\partial \mathrm{D}_1$ and $\partial \mathrm{D}_m$ are two horizontal boundaries of infinite extent (with $\partial \mathrm{D}_m$ below $\partial \mathrm{D}_1$), and $\hat{p}^+ = \hat{p}^+(\mathbf{x}, \omega)$ and $\hat{p}^- = \hat{p}^-(\mathbf{x}, \omega)$ are flux-normalized down going and up going fields, respectively (see Appendix A for the derivation). The terms 'down going' and 'up going' should be interpreted in a broad sense: for diffusion fields these terms mean 'decaying in the positive or negative x_3-direction, respectively'. The subscripts A and B refer to two independent states. Equation (2) holds for lossless as well as dissipative 3D inhomogeneous media. The underlying assumptions for equation (2) are that there are no sources between $\partial \mathrm{D}_1$ and $\partial \mathrm{D}_m$ and that in the region enclosed by these boundaries the medium parameters in states A and B are identical. Above $\partial \mathrm{D}_1$ and below $\partial \mathrm{D}_m$ the medium parameters and boundary conditions in states A and B need not be the same. The condition that $\partial \mathrm{D}_1$ and $\partial \mathrm{D}_m$ are horizontal boundaries can be relaxed. Frijlink 2007 shows that under certain conditions equation (2) also holds when $\partial \mathrm{D}_1$ and $\partial \mathrm{D}_m$ are smoothly curved boundaries.

Note that other variants of equation (2) exist, containing vertical derivatives of the down going and up going fields in one of the two states. This is the case, for example, when $\hat{p}^+$ and $\hat{p}^-$ represent down going and up going acoustic pressure fields. Since we consider flux-normalized fields these derivatives are absent in equation (2).

In the following, state B will represent the measured response of the real Earth, whereas state A will represent the new response of a redatumed source in an Earth with different boundary conditions, obtained by interferometry. Hence, state B is the actual state whereas state A is the desired state. First we discuss state B. Consider a dissipative 3D inhomogeneous Earth bounded by a free surface $\partial \mathrm{D}_0$, see Fig. 1(b). The source of the actual field at $\mathbf{x}_S$, with source spectrum $\hat{s}(\omega)$, is situated below $\partial \mathrm{D}_0$ and above the receivers. The receivers are located, for example, at the sea-bottom or in a horizontal borehole. The boundary $\partial \mathrm{D}_1$ is chosen an ϵ-distance below the receivers (e.g. just below the sea-bottom) and $\partial \mathrm{D}_m$ is chosen below all inhomogeneities. The measured field at the receivers is represented by a 2×1-vector $\hat{\mathbf{Q}}(\mathbf{x}, \mathbf{x}_S, \omega)$, containing for example the acoustic pressure and vertical component of the particle velocity, or the inline electric field and crossline magnetic field components. The quantities in this vector are continuous in the depth direction, hence, at $\partial \mathrm{D}_1$ (i.e. just below the receivers) we have the same $\hat{\mathbf{Q}}(\mathbf{x}, \mathbf{x}_S, \omega)$. This field vector is decomposed at $\partial \mathrm{D}_1$ into flux-normalized down going and up going fields, according to

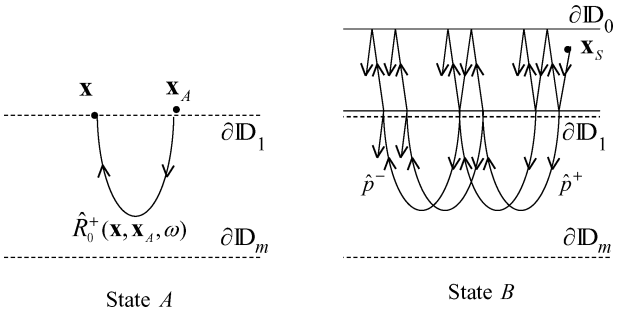

Figure 1. State A: the desired reflection response of the medium below $\partial \mathrm{D}_1$, for the situation of a non-reflecting half-space above $\partial \mathrm{D}_1$. State B: the actual response of the real earth, bounded by a free surface at $\partial \mathrm{D}_0$. The medium parameters exhibit dissipation, are 3D inhomogeneous functions of position, and below $\partial \mathrm{D}_1$ they are the same in both states.

$$\hat{\mathbf{P}}(\mathbf{x}, \mathbf{x}_S, \omega) = \hat{\boldsymbol{\mathcal{L}}}^{-1} \hat{\mathbf{Q}}(\mathbf{x}, \mathbf{x}_S, \omega), \tag{3}$$

where $\hat{\boldsymbol{\mathcal{L}}}^{-1}$ is a decomposition operator containing the medium parameters at $\partial \mathrm{D}_1$, and

$$\hat{\mathbf{P}}(\mathbf{x}, \mathbf{x}_S, \omega) = \begin{pmatrix} \hat{p}^+(\mathbf{x}, \mathbf{x}_S, \omega) \\ \hat{p}^-(\mathbf{x}, \mathbf{x}_S, \omega) \end{pmatrix}, \tag{4}$$

see Appendix B for details. Hence, in state B we have

$$\mathbf{x} \in \partial \mathrm{D}_1 : \quad \begin{cases} \hat{p}_B^+(\mathbf{x}, \omega) = \hat{p}^+(\mathbf{x}, \mathbf{x}_S, \omega), \\ \hat{p}_B^-(\mathbf{x}, \omega) = \hat{p}^-(\mathbf{x}, \mathbf{x}_S, \omega). \end{cases} \tag{5}$$

Since we chose $\partial \mathrm{D}_m$ below all inhomogeneities, there are only down going fields at $\partial \mathrm{D}_m$, hence

$$\mathbf{x} \in \partial \mathrm{D}_m : \quad \begin{cases} \hat{p}_B^+(\mathbf{x}, \omega) = \hat{p}^+(\mathbf{x}, \mathbf{x}_S, \omega), \\ \hat{p}_B^-(\mathbf{x}, \omega) = 0. \end{cases} \tag{6}$$

Note that the decomposition at $\partial \mathrm{D}_1$, as formulated by equation (3), requires that the field components in $\hat{\mathbf{Q}}(\mathbf{x}, \mathbf{x}_S, \omega)$ are properly sampled and that the (laterally varying) medium parameters at $\partial \mathrm{D}_1$ are known. When, in case of sea-bottom measurements, there is a very thin layer of soft sediment on top of a hard rock sea floor, then the parameters of the hard rock should be used in $\hat{\boldsymbol{\mathcal{L}}}^{-1}$. Schalkwijk, Wapenaar and Verschuur (2003) and Muijs, Robertsson and Holliger (2004) discuss adaptive decomposition schemes for sea-bottom seismic data, which estimate the sea-bottom parameters directly from the data by optimizing the decomposition result.

For the desired state A we replace the medium above $\partial \mathrm{D}_1$ by a non-reflecting half-space, see Fig. 1(a), which is

accomplished by choosing the medium parameters continuous across ∂D_1 and independent of x_3 above ∂D_1. We choose a point source for a down going field at $\mathbf{x}_A$ just above ∂D_1; the receivers are chosen at $\mathbf{x} \in \partial D_1$. We define $\hat{R}_0^+(\mathbf{x}, \mathbf{x}_A, \omega)$ as the reflection response of the medium below ∂D_1 with a source for a down going field at $\mathbf{x}_A$ and a receiver for an up going field at $\mathbf{x} \in \partial D_1$. The subscript '0' denotes that no multiples related to reflectors above ∂D_1 are included; the superscript '+' denotes that this is the response of a down going source field. For the down going and up going fields in state A we thus have

$$\mathbf{x} \in \partial D_1: \quad \begin{cases} \hat{p}_A^+(\mathbf{x}, \omega) = \delta(\mathbf{x}_H - \mathbf{x}_{H,A})\hat{s}_A(\omega), \\ \hat{p}_A^-(\mathbf{x}, \omega) = \hat{R}_0^+(\mathbf{x}, \mathbf{x}_A, \omega)\hat{s}_A(\omega), \end{cases} \tag{7}$$

where $\hat{s}_A(\omega)$ denotes the spectrum of the source at $\mathbf{x}_A$. We used the subscript H to denote the horizontal coordinates, hence $\mathbf{x}_H = (x_1, x_2)$ and $\mathbf{x}_{H,A} = (x_{1,A}, x_{2,A})$ (the latter denoting the horizontal coordinates of $\mathbf{x}_A$). At ∂D_m we have again only down going fields, hence

$$\mathbf{x} \in \partial D_m: \quad \begin{cases} \hat{p}_A^+(\mathbf{x}, \omega) = \hat{T}_0^+(\mathbf{x}, \mathbf{x}_A, \omega)\hat{s}_A(\omega), \\ \hat{p}_A^-(\mathbf{x}, \omega) = 0, \end{cases} \tag{8}$$

where $\hat{T}_0^+(\mathbf{x}, \mathbf{x}_A, \omega)$ is the transmission response of the medium between ∂D_1 and ∂D_m with a source at $\mathbf{x}_A$ and a receiver at $\mathbf{x} \in \partial D_m$. Substitution of equations (5)–(8) into equation (2), using source-receiver reciprocity [i.e., $\hat{R}_0^+(\mathbf{x}, \mathbf{x}_A, \omega) = \hat{R}_0^+(\mathbf{x}_A, \mathbf{x}, \omega)$] and dividing the result by $\hat{s}_A(\omega)$ gives

$$\hat{p}^-(\mathbf{x}_A, \mathbf{x}_S, \omega) = \int_{\partial D_1} \hat{R}_0^+(\mathbf{x}_A, \mathbf{x}, \omega)\hat{p}^+(\mathbf{x}, \mathbf{x}_S, \omega) \mathrm{d}^2\mathbf{x}. \tag{9}$$

This is an integral equation of the first kind for $\hat{R}_0^+(\mathbf{x}_A, \mathbf{x}, \omega)$. Note that $\hat{R}_0^+$ is the Fourier transform of an impulse response, whereas $\hat{p}^+$ and $\hat{p}^-$ are proportional to the source spectrum $\hat{s}(\omega)$ of the source at $\mathbf{x}_S$. For laterally invariant media equation (9) can easily be solved via a scalar division in the wavenumber-frequency domain. For 3D inhomogeneous media it can only be solved when the down going and up going fields $\hat{p}^+(\mathbf{x}, \mathbf{x}_S, \omega)$ and $\hat{p}^-(\mathbf{x}_A, \mathbf{x}_S, \omega)$ are available for a sufficient range of source positions $\mathbf{x}_S$. In matrix notation (Berkhout 1982), equation (9) can be written as

$$\hat{\mathsf{P}}^- = \hat{\mathsf{R}}_0^+ \hat{\mathsf{P}}^+. \tag{10}$$

For example, the columns of matrix $\hat{\mathsf{P}}^+$ contain $\hat{p}^+(\mathbf{x}, \mathbf{x}_S, \omega)$ for fixed $\mathbf{x}_S$ and variable $\mathbf{x}$ at ∂D_1, whereas the rows of this matrix contain $\hat{p}^+(\mathbf{x}, \mathbf{x}_S, \omega)$ for fixed $\mathbf{x}$ and variable $\mathbf{x}_S$ at ∂D_S, where ∂D_S represents the depth level of the sources. Inversion of equation (10) involves matrix inversion, according to

$$\hat{\mathsf{R}}_0^+ = \hat{\mathsf{P}}^-(\hat{\mathsf{P}}^+)^{-1} \tag{11}$$

(Wapenaar and Verschuur 1996). Note that equation (11) is the 3D equivalent of equation (1). The matrix inversion in equation (11) can be stabilized by least-squares inversion, according to

$$\hat{\mathsf{R}}_0^+ = \hat{\mathsf{P}}^-(\hat{\mathsf{P}}^+)^\dagger[(\hat{\mathsf{P}}^+)(\hat{\mathsf{P}}^+)^\dagger + \epsilon^2\mathsf{I}]^{-1}, \tag{12}$$

where the superscript † denotes transposition and complex conjugation, I is the identity matrix and ϵ is a small constant. Berkhout and Verschuur (2003) used a similar inversion for transforming surface-related multiples into primaries.

Equations (11) and (12) describe 3D interferometry-by-deconvolution. Schuster and Zhou (2006) derived an expression equivalent with equation (12) and called this least-squares redatuming. In the next section we generalize equations (9)–(12) for general vector fields.

Note that, due to the matrix inversion, 3D interferometry-by-deconvolution is by definition a multi-channel process. Unlike interferometry-by-correlation, it cannot be simplified to a single deconvolution for the situation of uncorrelated noise sources.

We conclude this section by comparing 3D interferometry-by-deconvolution with the virtual source method of Bakulin and Calvert (2006). We start by ignoring the inverse matrix in equation (12), according to

$$\hat{\mathsf{R}}_0^+ \approx \hat{\mathsf{P}}^-(\hat{\mathsf{P}}^+)^\dagger. \tag{13}$$

If we rewrite this equation again in integral form we obtain

$$\hat{R}_0^+(\mathbf{x}_A, \mathbf{x}, \omega) \approx \int_{\partial D_S} \hat{p}^-(\mathbf{x}_A, \mathbf{x}_S, \omega)\{\hat{p}^+(\mathbf{x}, \mathbf{x}_S, \omega)\}^* \mathrm{d}^2\mathbf{x}_S, \tag{14}$$

where the superscript $*$ denotes complex conjugation. Note that $\hat{R}_0^+$ is now proportional to the power spectrum $|\hat{s}(\omega)|^2$ of the sources at ∂D_S. Transforming equation (14) to the time domain yields

$$R_0^+(\mathbf{x}_A, \mathbf{x}, t) \approx \int_{\partial D_S} p^-(\mathbf{x}_A, \mathbf{x}_S, t) * p^+(\mathbf{x}, \mathbf{x}_S, -t)\, \mathrm{d}^2\mathbf{x}_S, \tag{15}$$

where $*$ denotes temporal convolution. The latter equation corresponds to the virtual source method of Bakulin and Calvert (2006). The integrand on the right-hand side represents the convolution of the up going field at $\mathbf{x}_A$ due to a source at $\mathbf{x}_S$ and the time-reversed down going field at $\mathbf{x}$ due to the same source. The integral is carried out along all sources at $\mathbf{x}_S \in \partial D_S$. The left-hand side is the response at $\mathbf{x}_A$ of a virtual source at $\mathbf{x}$. Bakulin and Calvert (2006) actually use a time-windowed version of $p^+(\mathbf{x}, \mathbf{x}_S, t)$, containing the first arrival (which is possible for wave fields but not for diffusion fields). The main effect of their method is the suppression of propagation distortions of the overburden. For comparison, inversion

of equation (9) not only removes the propagation distortions of the overburden, but also eliminates all multiple reflections related to all reflectors above ∂D_1, including the free surface ∂D_0.

INTERFEROMETRY-BY-DECONVOLUTION: 3D VECTOR VERSION

We generalize the approach discussed in the previous section. We replace the one-way scalar fields by general one-way vector fields (waves and/or diffusion fields) and we derive an 'interferometry-by-deconvolution' approach for these vector fields.

The vectorial extension of equation (2) for a dissipative 3D inhomogeneous medium reads

$$\int_{\partial D_1} \{(\hat{\mathbf{P}}_A^+)^t \hat{\mathbf{P}}_B^- - (\hat{\mathbf{P}}_A^-)^t \hat{\mathbf{P}}_B^+\}\, d^2\mathbf{x} = \int_{\partial D_m} \{(\hat{\mathbf{P}}_A^+)^t \hat{\mathbf{P}}_B^- - (\hat{\mathbf{P}}_A^-)^t \hat{\mathbf{P}}_B^+\}\, d^2\mathbf{x}, \tag{16}$$

where the superscript t denotes transposition and where vectors $\hat{\mathbf{P}}^+ = \hat{\mathbf{P}}^+(\mathbf{x}, \omega)$ and $\hat{\mathbf{P}}^- = \hat{\mathbf{P}}^-(\mathbf{x}, \omega)$ are flux-normalized down going and up going fields, respectively (see again Appendix A for the derivation). Following a similar derivation as in the previous section, using $\{\hat{\mathbf{R}}_0^+(\mathbf{x}, \mathbf{x}_A, \omega)\}^t = \hat{\mathbf{R}}_0^+(\mathbf{x}_A, \mathbf{x}, \omega)$ (Wapenaar, Thorbecke and Draganov 2004), we obtain for the configuration of Fig. 1

$$\hat{\mathbf{P}}^-(\mathbf{x}_A, \mathbf{x}_S, \omega) = \int_{\partial D_1} \hat{\mathbf{R}}_0^+(\mathbf{x}_A, \mathbf{x}, \omega)\hat{\mathbf{P}}^+(\mathbf{x}, \mathbf{x}_S, \omega) d^2\mathbf{x}. \tag{17}$$

A similar expression was derived for electromagnetic fields by Amundsen and Holvik (2004, Processing electromagnetic data, Patent GB2415511) and for elastodynamic wave fields by Holvik and Amundsen (2005). In equation (17) $\hat{\mathbf{P}}^+(\mathbf{x}, \mathbf{x}_S, \omega)$ and $\hat{\mathbf{P}}^-(\mathbf{x}_A, \mathbf{x}_S, \omega)$ are obtained from a field vector $\hat{\mathbf{Q}}(\mathbf{x}, \mathbf{x}_S, \omega)$ at ∂D_1 by decomposition, see Appendix C for details. Vector $\hat{\mathbf{Q}}(\mathbf{x}, \mathbf{x}_S, \omega)$ contains, for example, an elastodynamic or electromagnetic field, measured by multicomponent receivers. The multicomponent sources for these fields are located at $\mathbf{x}_S \in \partial D_S$. $\hat{\mathbf{R}}_0^+(\mathbf{x}_A, \mathbf{x}, \omega)$ is a matrix containing the reflection responses of the medium below ∂D_1 with multicomponent sources for down going fields at $\mathbf{x} \in \partial D_1$ and multicomponent receivers for up going fields at $\mathbf{x}_A$. For example, for the situation of elastodynamic waves, vectors $\hat{\mathbf{P}}^+$ and $\hat{\mathbf{P}}^-$ in equation (17) are defined as

$$\hat{\mathbf{P}}^+ = \begin{pmatrix} \hat{\Phi}^+ \\ \hat{\Psi}^+ \\ \hat{\Upsilon}^+ \end{pmatrix} \quad \text{and} \quad \hat{\mathbf{P}}^- = \begin{pmatrix} \hat{\Phi}^- \\ \hat{\Psi}^- \\ \hat{\Upsilon}^- \end{pmatrix}, \tag{18}$$

where $\hat{\Phi}^\pm$, $\hat{\Psi}^\pm$ and $\hat{\Upsilon}^\pm$ represent flux-normalized down going and up going P, S_1 and S_2 waves, respectively. Moreover, for this situation matrix $\hat{\mathbf{R}}_0^+(\mathbf{x}_A, \mathbf{x}, \omega)$ is written as

$$\hat{\mathbf{R}}_0^+(\mathbf{x}_A, \mathbf{x}, \omega) = \begin{pmatrix} \hat{R}^+_{\phi,\phi} & \hat{R}^+_{\phi,\psi} & \hat{R}^+_{\phi,\upsilon} \\ \hat{R}^+_{\psi,\phi} & \hat{R}^+_{\psi,\psi} & \hat{R}^+_{\psi,\upsilon} \\ \hat{R}^+_{\upsilon,\phi} & \hat{R}^+_{\upsilon,\psi} & \hat{R}^+_{\upsilon,\upsilon} \end{pmatrix} (\mathbf{x}_A, \mathbf{x}, \omega), \tag{19}$$

(no summation convention) where $\hat{R}^+_{p,q}(\mathbf{x}_A, \mathbf{x}, \omega)$ denotes the reflection response of the medium below ∂D_1 in terms of a down going q-type wave field at $\mathbf{x}$ and a reflected p-type wave field at $\mathbf{x}_A$.

Equation (17) is an integral equation of the first kind for $\hat{\mathbf{R}}_0^+(\mathbf{x}_A, \mathbf{x}, \omega)$. For 3D inhomogeneous media it can only be solved when the down going and up going fields $\hat{\mathbf{P}}^+(\mathbf{x}, \mathbf{x}_S, \omega)$ and $\hat{\mathbf{P}}^-(\mathbf{x}_A, \mathbf{x}_S, \omega)$ are available for a sufficient range of source positions $\mathbf{x}_S$ and for a sufficient number of independent source components at each source position. To be more specific, since $\hat{\mathbf{P}}^+$ and $\hat{\mathbf{P}}^-$ are $\frac{K}{2} \times 1$ vectors (see Appendix A), $\frac{K}{2}$ independent source components are needed to solve equation (17) uniquely. For example, when for the elastodynamic situation three orthogonal forces are employed at each source position, equation (17) can be solved (Holvik and Amundsen 2005). The least-squares solution procedure for the general $\frac{K}{2} \times \frac{K}{2}$ reflection response matrix is similar to that described in the previous section, in particular by equations (10)–(12).

NUMERICAL EXAMPLE OF CSEM INTERFEROMETRY

We illustrate interferometry-by-deconvolution with a numerical example. We choose to apply it to simulated controlled-source electromagnetic (CSEM) data because this best demonstrates the ability of the proposed method to deal with dissipation. Although the spatial resolution of CSEM data is much lower than that of seismic data, the main advantage of CSEM prospecting is its power to detect a hydrocarbon accumulation in a reservoir due to its high conductivity contrast (Ellingsrud *et al.* 2002; Moser *et al.* 2006). Amundsen *et al.* (2006) showed that decomposition of CSEM data into down going and up going fields improves the detectability of hydrocarbon reservoirs. Below we show that the combination of decomposition and interferometry-by-deconvolution not only improves the detectability but also results in improved quantitative information about the reservoir parameters.

The model consists of a plane layered Earth. The 2D TM-mode (see Table B1) is modeled as a two-dimensional approximation of the CSEM method as applied in Seabed Logging applications. The model is shown in Fig. 2, where the seawater

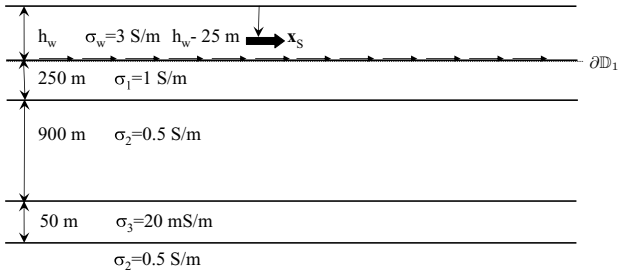

Figure 2 The configuration with a reservoir-type layer at 1150 m below the sea bottom and a water layer with variable thickness: $h_w = 50$ m or $h_w = 500$ m. The source is 25 m above the sea bottom and the receiver array is located at the sea bottom.

layer contains an inline electric current source at 25 m above the sea bottom. The receivers are located at the sea bottom with a total extent of 40 km. The water layer is modeled with variable thickness and we take the values of 50 m as a model for a shallow sea and of 500 m as a model of a deep sea. The seawater has a conductivity of $\sigma_w = 3$ S/m. Below the sea bottom there is a layer with a conductivity of $\sigma_1 = 1$ S/m with a thickness of 250 m. This is followed by a half-space with $\sigma_2 = 0.5$ S/m, which is intersected after 900 m by a reservoir-type layer with a thickness of 50 m and a conductivity of $\sigma_3 = 20$ mS/m. Note that the top of this reservoir layer is located at 1150 m below the sea bottom.

For the modeling, a unit strength AC current with an oscillation frequency of 0.25 Hz, a receiver separation of 40 m and a total offset range of 40 km have been used. The array measures both the horizontal electric and magnetic field components ($\hat{E}_1$ and $\hat{H}_2$) as depicted in Fig. 3 for the two water depths of 50 m and 500 m for the situation with and without the reservoir layer. It can be observed that for small offsets, the in-line electric field component shows more decay as a function of offset than the cross-line magnetic field component.

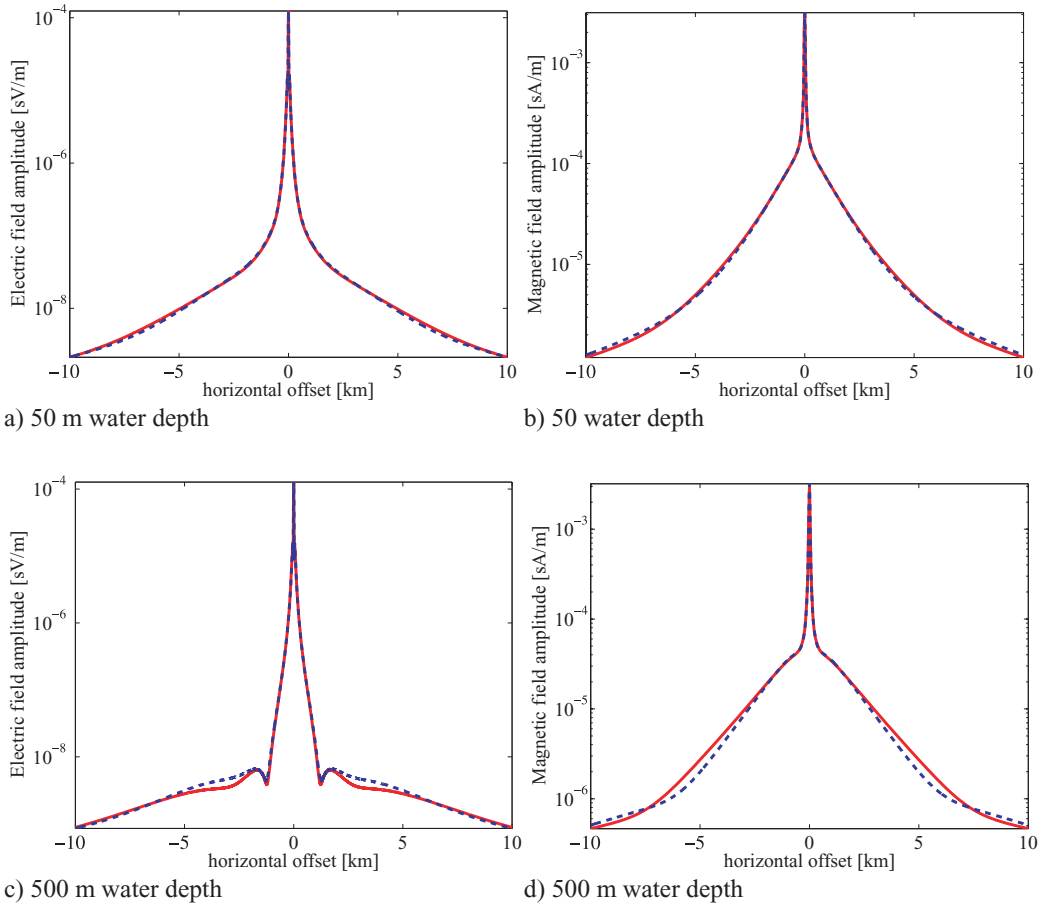

Figure 3 The electromagnetic field, at f = 0.25 Hz, at the sea bottom. (a) The electric and (b) the magnetic field amplitudes for a water depth $h_w = 50$ m. (c) The electric and (d) magnetic field amplitudes for a water depth of $h_w = 500$ m. The red and blue curves represent the situation with and without the reservoir layer.

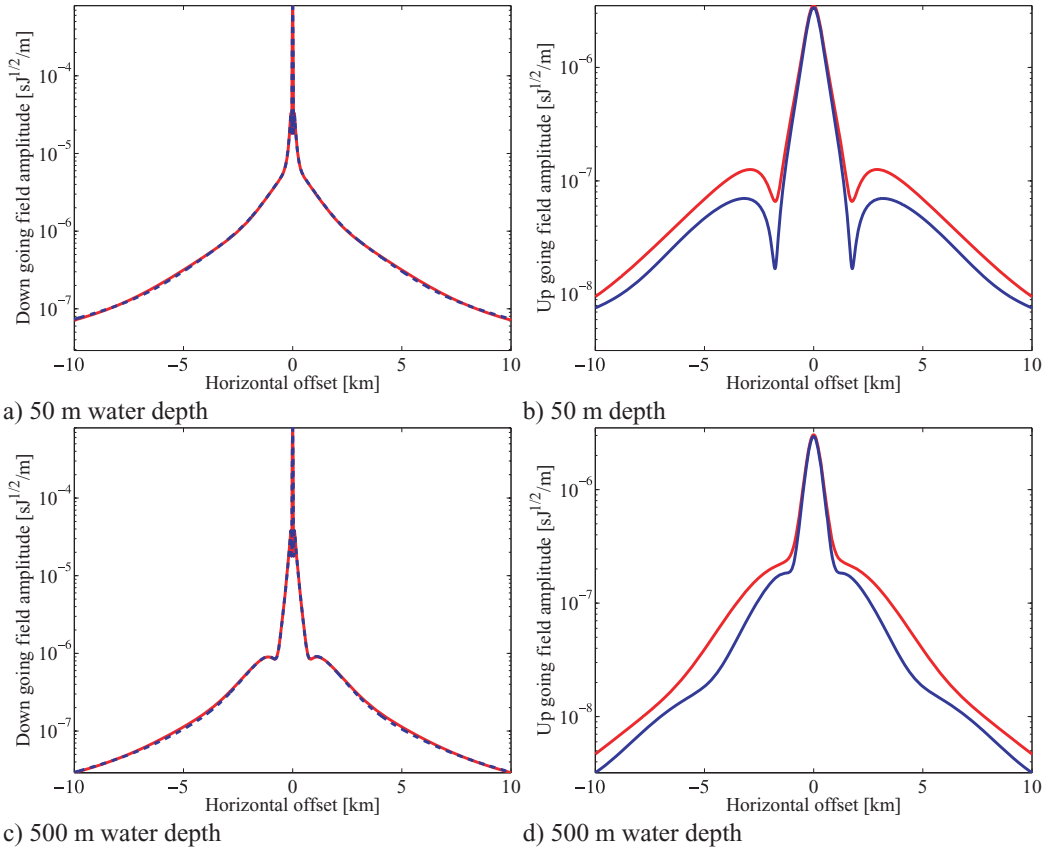

Figure 4 Decomposition of 2D TM field at f = 0.25 Hz just below the sea bottom. (a) Down going field and (b) up going field for a water depth $h_w = 50$ m. (c) Down going field and (d) up going field for a water depth $h_w = 500$ m. The red and blue curves represent the situation with and without the reservoir layer, respectively. In (a) and (c) the blue curves are hidden by the red curves.

For large offset the situation is reversed. For the deep sea the difference between the presence and absence of the reservoir layer is more pronounced than in the shallow sea situation. We can decompose the measured fields into flux-normalized down going and up going fields (equation 3). The decomposition is carried out using the parameters of the first layer below the sea bottom. Hence, the resulting down going and up going fields correspond to the fields just below the sea bottom. Both are shown in Fig. 4 for the two water depths of 50 m and 500 m for the situation with and without the reservoir layer. The effect of the reservoir response is clearly visible in the up going fields for offsets larger than 2 km in the shallow sea and for offsets larger than 1 km in the deep sea. It is almost not visible in the down going field (except at offsets larger than 4 km, indicating that its multiple interaction with the water layer is very small). The sharp minima that occur in the up going fields correspond to sign changes in the real and imaginary parts. By comparing Fig. 4b with 4d it can be seen that the shallow water layer has a strong effect on the amplitude and shape of the

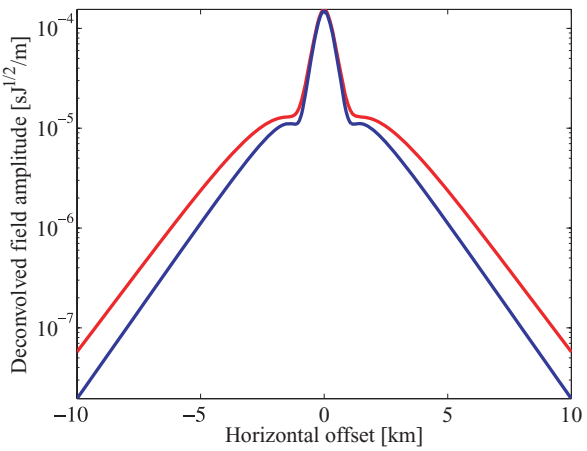

Figure 5 The reflection response $\hat{R}_0^+(\mathbf{x}_A, \mathbf{x}, \omega)$ at f = 0.25 Hz just below the sea bottom, obtained by interferometry-by-deconvolution. The result is independent of the water depth. The red and blue curves represent the situation with and without the reservoir layer, respectively.

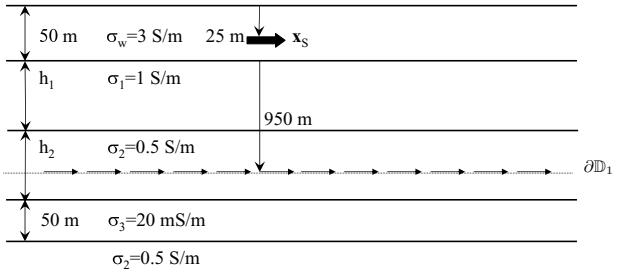

Figure 6 The configuration with a reservoir-type layer at 1150 m below the sea bottom and a water layer with a fixed thickness of 50 m. The source is 25 m above the sea bottom and the receiver array is located in a horizontal borehole 950 m below the sea bottom and 200 m above the top of the reservoir layer. The Earth layers have variable thicknesses: $h_1 = 250$ m and $h_2 = 900$ m, or $h_1 = 900$ m and $h_2 = 250$m.

up going field, which makes quantitative analysis of the reservoir parameters very difficult. This effect can be eliminated by performing interferometry-by-deconvolution, that is, by solving equation (9) for $\hat{R}_0^+(\mathbf{x}_A, \mathbf{x}, \omega)$. Since in this example the medium is horizontally layered, we solve equation (9) by applying a division in the wavenumber-frequency domain and transforming the result back to the space-frequency domain. The result is shown in Fig. 5 for the situation with and without the reservoir layer. After this step the effect of the water layer has been completely removed and therefore this result is independent of the water depth in the original model. It is as if the upper most Earth layer now extends upward to infinity. Moreover, note that in $\hat{R}_0^+(\mathbf{x}_A, \mathbf{x}, \omega)$ the original source has been replaced by a source at the receiver level, while only the reflection response of the medium below the sea bottom is retained. Hence, the strong direct field has also been eliminated. In theory, this procedure solves the shallow sea problem of the seabed logging method. It should be noted that we considered

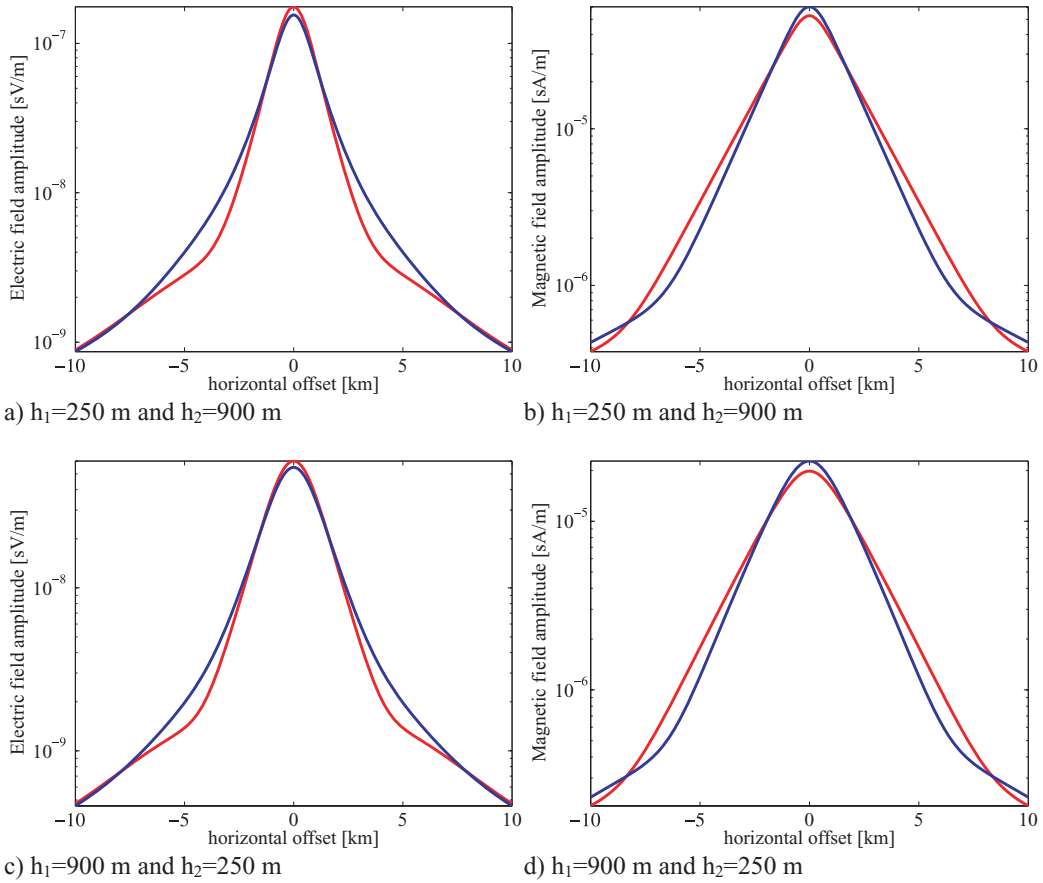

Figure 7 Electric and magnetic field amplitudes, at f = 0.25 Hz, in a horizontal borehole 200 m above the top of the reservoir layer. (a) The electric field and (b) the magnetic field for $h_1 = 250$ m and $h_2 = 900$ m. (c) The electric field and (d) the magnetic field for $h_1 = 900$ m and $h_2 = 250$ m. The red and blue curves represent the situation with and without the reservoir layer.

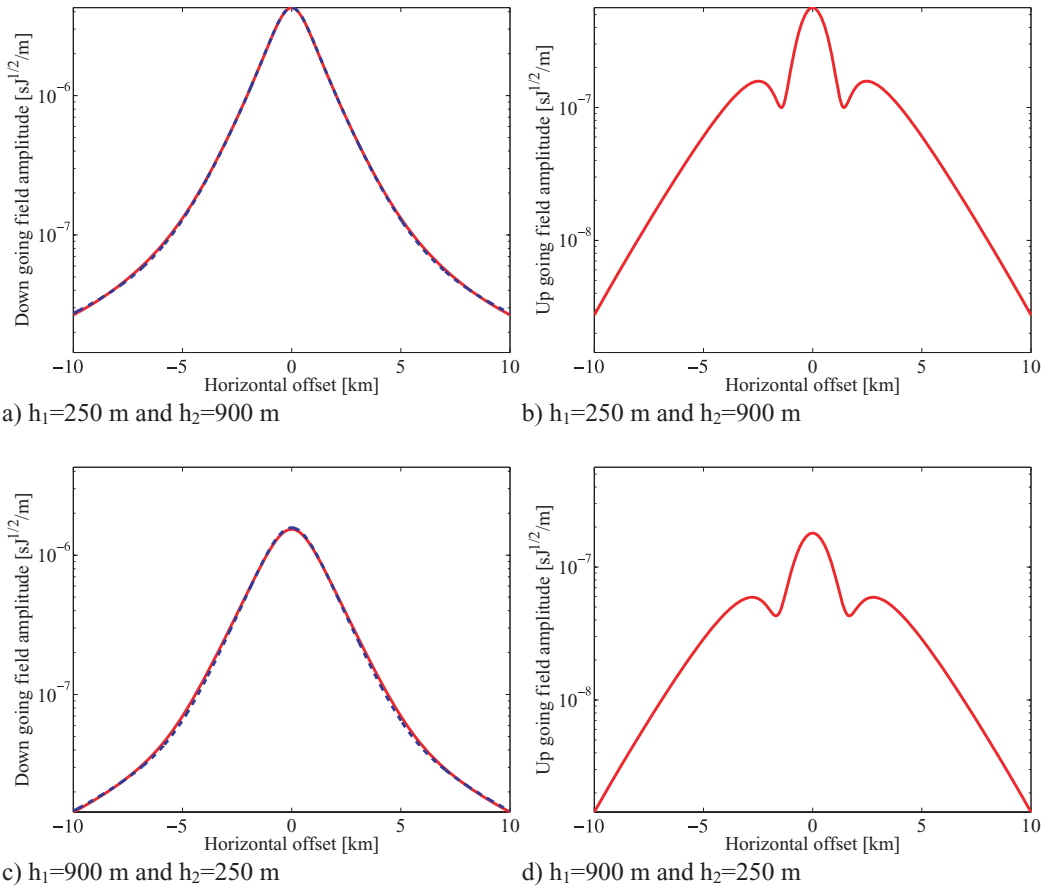

Figure 8 Decomposition of 2D TM field at f = 0.25 Hz in a horizontal borehole 200 m above the top of the reservoir layer. (a) Down going field and (b) up going field for $h_1 = 250$ m and $h_2 = 900$ m. (c) Down going field and (d) up going field for $h_1 = 900$ m and $h_2 = 250$ m. The red and blue curves represent the situation with and without the reservoir layer, respectively. In (a) and (c) the blue curves are hidden by the red curves. In (b) and (d) there are only red curves since in the situation without reservoir layer there are no up going fields.

an ideal situation of well sampled data, measured with high precision and no noise added.

When a horizontal borehole is available at depth we can perform these steps again, thereby removing the direct field and all overburden effects, leaving only the reservoir response. The model is the same as in Fig. 2, but now the water depth is maintained constant at 50 m, while the first two Earth layers have in the first example thicknesses of $h_1 = 250$ m and $h_2 = 900$ m, and in the second example $h_1 = 900$ m and $h_2 = 250$ m (keeping the total thickness fixed). The receiver array is located in a horizontal borehole at 950 m below the sea bottom, 200 m above the top of the reservoir, as indicated in Fig. 6. Again we assume that $\hat{E}_1$ and $\hat{H}_2$ are available so that decomposition is possible. The fields are modelled with a receiver separation of 160 m and the results are shown in Fig. 7 for the situation with a water depth of 50 m, with and without reservoir layer and with a first layer of 250 m and a second layer of 900 m

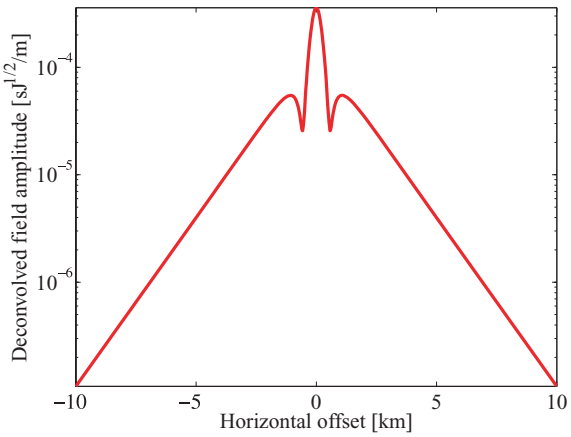

Figure 9 The reflection response $\hat{R}_0^+(\mathbf{x}_A, \mathbf{x}, \omega)$ at f=0.25 Hz in a horizontal borehole 200 m above the top of the reservoir layer, obtained by interferometry-by-deconvolution. The result is independent of the overburden.

as well as the reversed situation. The decomposition result is shown in Fig. 8, where the up going fields in 8b and 8d clearly demonstrate the detectability of the reservoir layer. Note that these up going fields have similar shapes, but their field amplitudes differ by a factor of 4. This can be understood from the fact that the interaction between the reservoir and the interface above the reservoir plays a more prominent role in the up going field in the second example (Fig. 8d) where the interface is located 250 m above the top of the reservoir and only 50 m above the receivers. Figure 9 shows $\hat{R}_0^+(\mathbf{x}_A, \mathbf{x}, \omega)$, obtained by interferometry-by-deconvolution. Sources as well as receivers are now in the horizontal borehole, 200 m above the top of the reservoir layer. This result is independent of the overburden in the original model. In theory it is the exact reflection response of the reservoir layer as if it were embedded in a homogeneous medium with a conductivity of $\sigma_2 = 0.5$ S/m.

CONCLUSIONS

One of the main assumptions in most seismic interferometry schemes is that the medium is lossless. We have shown that this assumption can be circumvented when the crosscorrelation procedure (the central step in seismic interferometry) is replaced by a multi-dimensional deconvolution procedure. We derived an algorithm for 'interferometry-by-deconvolution' for the situation of sources at or below the Earth's surface and multicomponent receivers at depth, for example at the seabottom or in a horizontal borehole. The proposed algorithm not only moves the source to the receiver depth level ('source redatuming'), but also changes the boundary conditions in such a way that the overburden becomes non-reflecting. The result is a reflection response observed relatively close to the target, without the disturbing effects of the overburden. As in all interferometry approaches, no knowledge of the medium is required, except at the depth level of the receivers, where a decomposition into down going and up going fields takes place.

An important application of 'interferometry-by-deconvolution' is removing the air/sea interface and the direct field in CSEM data. The two main factors that complicate standard CSEM data processing are the presence of the direct field and, for shallow seas, the presence of the field reflected at the sea surface (effect of the air wave). Both effects interfere with the subsurface response in the measurements. Due to the diffuse character of the EM fields the direct field and the effect of the air wave cannot be separated in the measurement by time windowing. The method we propose here removes both effects, thereby in theory solving the shallow sea problem of CSEM applications. For deep receivers, the method removes the direct field and all overburden effects.

ACKNOWLEDGEMENTS

This work is supported by the Netherlands Research Centre for Integrated Solid Earth Science (ISES) and the sponsors of the CWP project. We thank the reviewers Anton Ziolkowski and Lasse Amundsen for their constructive comments.

REFERENCES

Amundsen L. 1999. Elimination of free surface-related multiples without need of the source wavelet. 69th SEG meeting, Houston, Texas, USA, Expanded Abstracts, 1064–1067.

Amundsen L., Løseth L., Mittet R., Ellingsrud S. and Ursin B. 2006. Decomposition of electromagnetic fields into upgoing and downgoing components. *Geophysics* **71**, G211–G223.

Anno P., Cohen J.K. and Bleistein N. 1992. Waves and rays in acoustic variable density media. 62nd SEG meeting, New Orleans, Louisiana, USA, Expanded Abstracts, 1332–1336.

Bakulin A. and Calvert R. 2006. The virtual source method: Theory and case study. *Geophysics* **71**, SI139–SI150.

Berkhout A.J. 1982. *Seismic Migration. Imaging of Acoustic Energy by Wave Field Extrapolation*. Elsevier.

Berkhout A.J. and Verschuur D.J. 2003. Transformation of multiples into primary reflections. 73rd SEG meeting, Dallas, Texas, USA, Expanded Abstracts, 1925–1928.

Corones J.P., Davison M.E. and Krueger R.J. 1983. Direct and inverse scattering in the time domain via invariant imbedding equations. *Journal of the Acoustical Society of America* **74**, 1535–1541.

Corones J.P., Kristensson G., Nelson P. and Seth D. 1992. *Invariant Imbedding and Inverse Problems*. SIAM, Philadelphia.

de Hoop M.V. 1992. Directional decomposition of transient acoustic wave fields. PhD thesis, Delft University of Technology, The Netherlands.

de Hoop M.V. 1996. Generalization of the Bremmer coupling series. *Journal of Mathematical Physics* **37**, 3246–3282.

Draganov D., Wapenaar K., Mulder W., Singer J. and Verdel A. 2007. Retrieval of reflections from seismic background-noise measurements. *Geophysical Research Letters* **34**, L04305-1–L04305-4.

Ellingsrud S., Eidesmo T., Johansen S., Sinha M.C., MacGregor L.M. and Constable S. 2002. Remote sensing of hydrocarbon layers by seabed logging (SBL): Results from a cruise offshore Angola. *The Leading Edge* **21**, 972–982.

Fishman L. 1993. One-way propagation methods in direct and inverse scalar wave propagation modeling. *Radio Science* **28**, 865–876.

Fishman L., McCoy J.J. and Wales S.C. 1987. Factorization and path integration of the Helmholtz equation: Numerical algorithms. *Journal of the Acoustical Society of America* **81**, 1355–1376.

Frasier C.W. 1970. Discrete time solution of plane P-SV waves in a plane layered medium. *Geophysics* **35**, 197–219.

Frijlink M.O. 2007. Seismic redatuming with transmission loss correction in complex media. PhD thesis, Delft University of Technology, The Netherlands.

Gerstoft P., Sabra K.G., Roux P., Kuperman W.A. and Fehler M.C. 2006. Green's functions extraction and surface-wave tomography from microseisms in southern California. *Geophysics* **71**, SI23–SI31.

Godin O.A. 2006. Recovering the acoustic Green's function from ambient noise cross correlation in an inhomogeneous moving medium. *Physical Review Letters* **97**, 054301-1–054301-4.

Haartsen M.W. and Pride S.R. 1997. Electroseismic waves from point sources in layered media. *Journal of Geophysical Research* **102**, 24745–24769.

Haines A.J. and de Hoop M.V. 1996. An invariant imbedding analysis of general wave scattering problems. *Journal of Mathematical Physics* **37**, 3854–3881.

Holvik E. and Amundsen L. 2005. Elimination of the overburden response from multicomponent source and receiver seismic data, with source designature and decomposition into PP-, PS-, SP-, and SS-wave responses. *Geophysics* **70**, S43–S59.

Larose E., Margerin L., Derode A., van Tiggelen B., Campillo M., Shapiro N., Paul A., Stehly L. and Tanter M. 2006. Correlation of random wave fields: An interdisciplinary review. *Geophysics* **71**, SI11–SI21.

Mehta K., Snieder R. and Graizer V. 2007. Extraction of near-surface properties for a lossy layered medium using the propagator matrix. *Geophysical Journal International* **169**, 271–280.

Messiah A. 1962. *Quantum Mechanics, Volume II*. North-Holland Publishing Company, Amsterdam.

Moser J., Poupon M., Meyer H.-J., Wojcik C., Rosenquist M., Adejonwo A. and Smit D. 2006. Integration of electromagnetic and seismic data to assess residual gas risk in the toe-thrust belt of deepwater Niger Delta. *The Leading Edge* **25**, 977–982.

Muijs R., Robertsson J.O.A. and Holliger K. 2004. Data-driven adaptive decomposition of multicomponent seabed recordings. *Geophysics* **69**, 1329–1337.

Pride S.R. and Haartsen M.W. 1996. Electroseismic wave properties. *Journal of the Acoustical Society of America* **100**, 1301–1315.

Reid W.T. 1972. *Riccati Differential Equations*. Academic Press, New York.

Riley D.C. and Claerbout J.F. 1976. 2D multiple reflections. *Geophysics* **41**, 592–620.

Ruigrok E., Draganov D. and Wapenaar K. 2008. Global-scale seismic interferometry: theory and numerical examples. *Geophysical Prospecting*, this issue.

Schalkwijk K.M., Wapenaar C.P.A. and Verschuur D.J. 2003. Adaptive decomposition of multicomponent ocean-bottom seismic data into downgoing and upgoing P- and S-waves. *Geophysics* **68**, 1091–1102.

Schuster G.T. and Zhou M. 2006. A theoretical overview of model-based and correlation-based redatuming methods. *Geophysics* **71**, SI103–SI110.

Schuster G.T., Yu J., Sheng J. and Rickett J. 2004. Interferometric/daylight seismic imaging. *Geophysical Journal International* **157**, 838–852.

Slob E., Draganov D. and Wapenaar K. 2006. GPR without a source. *Eleventh International Conference on Ground Penetrating Radar*, p. ANT.6.

Slob E., Draganov D. and Wapenaar K. 2007. Interferometric electromagnetic Green's functions representations using propagation invariants. *Geophysical Journal International* **169**, 60–80.

Snieder R. 2004. Extracting the Green's function from the correlation of coda waves: A derivation based on stationary phase. *Physical Review E* **69**, 046610-1–046610-8.

Snieder R. 2006. Retrieving the Green's function of the diffusion equation from the response to a random forcing. *Physical Review E* **74**, 046620-1–046620-4.

Snieder R. 2007. Extracting the Green's function of attenuating acoustic media from uncorrelated waves. *Journal of the Acoustical Society of America* **121**, 2637–2643.

Snieder R., Sheiman J. and Calvert R. 2006. Equivalence of the virtual-source method and wave-field deconvolution in seismic interferometry. *Physical Review E* **73**, 066620-1–066620-9.

Snieder R., Wapenaar K. and Wegler U. 2007. Unified Green's function retrieval by cross-correlation; connection with energy principles. *Physical Review E* **75**, 036103-1–036103-14.

Ursin B. 1983. Review of elastic and electromagnetic wave propagation in horizontally layered media. *Geophysics* **48**, 1063–1081.

van Manen D-J., Robertsson J.O.A. and Curtis A. 2005. Modeling of wave propagation in inhomogeneous media. *Physical Review Letters* **94**, 164301-1–164301-4.

Wapenaar C.P.A. and Verschuur D.J. 1996. Processing of ocean bottom data. In: *The Dolphin Project, Volume I*, pp. 6.1–6.26. Delft University of Technology.

Wapenaar C.P.A., Dillen M.W.P. and Fokkema J.T. 2001. Reciprocity theorems for electromagnetic or acoustic one-way wave fields in dissipative inhomogeneous media. *Radio Science* **36**, 851–863.

Wapenaar K. 2006. Nonreciprocal Green's function retrieval by cross correlation. *Journal of the Acoustical Society of America* **120**, EL7–EL13.

Wapenaar K., Fokkema J., Dillen M., and Scherpenhuijsen P. 2000. One-way acoustic reciprocity and its applications in multiple elimination and time-lapse seismics. 70th SEG meeting, Calgary, Canada, Expanded Abstracts, 2377–2380.

Wapenaar K., Thorbecke J. and Draganov D. 2004. Relations between reflection and transmission responses of three-dimensional inhomogeneous media. *Geophysical Journal International* **156**, 179–194.

Wapenaar K., Slob E. and Snieder R. 2006. Unified Green's function retrieval by cross correlation. *Physical Review Letters* **97**, 234301-1–234301-4.

Weaver R.L. and Lobkis O.I. 2001. Ultrasonics without a source: Thermal fluctuation correlations at MHz frequencies. *Physical Review Letters* **87**, 134301-1–134301-4.

Weaver R.L. and Lobkis O.I. 2004. Diffuse fields in open systems and the emergence of the Green's function (L). *Journal of the Acoustical Society of America* **116**, 2731–2734.

Woodhouse J.H. 1974. Surface waves in a laterally varying layered structure. *Geophysical Journal of The Royal Astronomical Society* **37**, 461–490.

Ziolkowski A., Taylor D.B. and Johnston R.G.K. 1998. Multiple wavefields: separating incident from scattered, up from down, and primaries from multiples. 68th SEG meeting, New Orleans, Louisiana, USA, Expanded Abstracts, 1499–1502.

APPENDIX A: ONE-WAY RECIPROCITY THEOREMS FOR 3D INHOMOGENEOUS DISSIPATIVE MEDIA

We derive the convolution-type reciprocity theorems for one-way scalar and vector fields (equations 2 and 16). There are two approaches for deriving these theorems. The first approach starts with decomposing the equation for the total field into one-way equations, followed by deriving reciprocity theorems for the one-way fields. The advantage of this approach is that it leads to relatively simple expressions, even when the medium parameters in both states are different and sources are present in the considered domain (e.g. Wapenaar, Dillen and Fokkema 2001). The disadvantage is that for the situation of a 3D inhomogeneous medium (dissipative or lossless), exact derivations exist only for scalar fields, whereas in the derivations for vector fields approximations are made throughout the domain of the application.In the second approach the order of steps is reversed, hence, it starts with deriving a reciprocity theorem for the total field, followed by decomposition of the fields in this reciprocity theorem into one-way fields. The first step in this approach is exact for scalar as well as vector fields in 3D inhomogeneous media (dissipative or lossless). For the special situation that the medium parameters in both states are identical and the considered domain is source-free, this reciprocity theorem reduces to an integral over the boundary of the domain. Hence, for the subsequent decomposition step, approximations only need to be made at this boundary. When the medium is laterally invariant at the boundary of the domain, no approximations need to be made at all. Since in this paper we consider the situation of a source-free domain with identical medium parameters in both states (i.e. the domain between $\partial\mathrm{D}_1$ and $\partial\mathrm{D}_m$ in Fig. 1), we follow the second approach.

Our starting point is the following equation

$$\frac{\partial \hat{\mathbf{Q}}}{\partial x_3} = \hat{\boldsymbol{\mathcal{A}}}\hat{\mathbf{Q}}, \tag{A1}$$

where $\hat{\mathbf{Q}} = \hat{\mathbf{Q}}(\mathbf{x}, \omega)$ is a $K \times 1$ field vector and $\hat{\boldsymbol{\mathcal{A}}} = \hat{\boldsymbol{\mathcal{A}}}(\mathbf{x}, \omega)$ a $K \times K$ operator matrix containing a particular combination of the medium parameters and the horizontal differentiation operators $\partial/\partial x_\alpha$ for $\alpha = 1, 2$. This equation holds for acoustic wave fields in fluids ($K = 2$), electromagnetic wave and/or diffusion fields in matter ($K = 4$, Reid 1972), elastodynamic fields in solids ($K = 6$, Woodhouse 1974), poroelastic waves in porous solids ($K = 8$) and seismoelectric waves in porous solids ($K = 12$, Pride and Haartsen 1996; Haartsen and Pride 1997). Vector $\hat{\mathbf{Q}}$ and operator matrix $\hat{\boldsymbol{\mathcal{A}}}$ are specified for some of these cases in Appendices B and C.

We consider a dissipative 3D inhomogeneous medium in a domain D enclosed by two horizontal boundaries $\partial\mathrm{D}_1$ and $\partial\mathrm{D}_m$, with outward pointing normal vector $\mathbf{n} = (0, 0, -1)$ on $\partial\mathrm{D}_1$ and $\mathbf{n} = (0, 0, +1)$ on $\partial\mathrm{D}_m$, and a cylindrical boundary $\partial\mathrm{D}_{\mathrm{cyl}}$ with a vertical axis and normal vector $\mathbf{n} = (n_1, n_2, 0)$, see Fig. 10. In the following we assume that the horizontal boundaries $\partial\mathrm{D}_1$ and $\partial\mathrm{D}_m$ are of infinite extent (which implies that the radius of the cylindrical boundary $\partial\mathrm{D}_{\mathrm{cyl}}$ is also infinite), the domain D between boundaries $\partial\mathrm{D}_1$ and $\partial\mathrm{D}_m$ is source-free and the medium parameters in states *A* and *B* are identical in this domain.

For an arbitrary operator matrix $\hat{\boldsymbol{\mathcal{U}}}$ containing $\partial/\partial x_\alpha$ for $\alpha = 1, 2$, we introduce the transposed $\hat{\boldsymbol{\mathcal{U}}}^t$ via

$$\int_{\mathbb{R}^2} (\hat{\boldsymbol{\mathcal{U}}}\mathbf{f})^t \mathbf{g}\, \mathrm{d}^2\mathbf{x}_H = \int_{\mathbb{R}^2} \mathbf{f}^t (\hat{\boldsymbol{\mathcal{U}}}^t \mathbf{g})\, \mathrm{d}^2\mathbf{x}_H, \tag{A2}$$

where $\mathbf{f} = \mathbf{f}(\mathbf{x}_H)$ and $\mathbf{g} = \mathbf{g}(\mathbf{x}_H)$ are arbitrary square-integrable $K \times 1$ vector functions. According to this equation, $\hat{\boldsymbol{\mathcal{U}}}^t$ is a transposed matrix, containing transposed operators (with

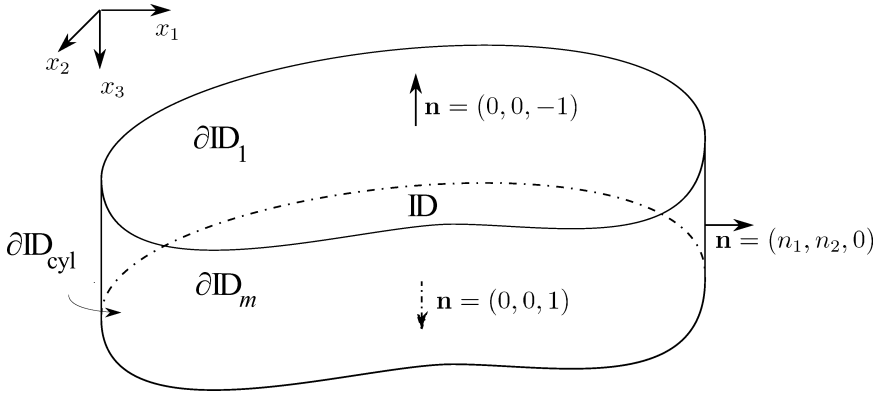

Figure 10 Configuration for the reciprocity theorems.

$(\partial/\partial x_\alpha)^t = -\partial/\partial \setminus x_\alpha$, which follows from the rules for partial integration). The operator matrix $\hat{\boldsymbol{\mathcal{A}}}$ is organized such that it obeys the following symmetry relation

$$\hat{\boldsymbol{\mathcal{A}}}^t\mathbf{N} = -\mathbf{N}\hat{\boldsymbol{\mathcal{A}}}, \tag{A3}$$

with

$$\mathbf{N} = \begin{pmatrix} \mathbf{O} & \mathbf{I} \\ -\mathbf{I} & \mathbf{O} \end{pmatrix}, \tag{A4}$$

where $\mathbf{I}$ and $\mathbf{O}$ are $\frac{K}{2} \times \frac{K}{2}$ identity and null matrices (note that $K = 2$ for scalar fields, hence $\mathbf{I} = 1$ and $\mathbf{O} = 0$).

We define an interaction quantity $\frac{\partial}{\partial x_3}\{\hat{\mathbf{Q}}_A^t\mathbf{N}\hat{\mathbf{Q}}_B\}$, where subscripts A and B denote two independent states. Applying the product rule for differentiation and substituting equation (A1) we obtain

$$\frac{\partial}{\partial x_3}\left\{\hat{\mathbf{Q}}_A^t\mathbf{N}\hat{\mathbf{Q}}_B\right\} = (\hat{\boldsymbol{\mathcal{A}}}\hat{\mathbf{Q}}_A)^t\mathbf{N}\hat{\mathbf{Q}}_B + \hat{\mathbf{Q}}_A^t\mathbf{N}\hat{\boldsymbol{\mathcal{A}}}\hat{\mathbf{Q}}_B. \tag{A5}$$

Integrating over $\mathbf{x}_H$ and using equation (A2) gives

$$\int_{\mathbb{R}^2} \frac{\partial}{\partial x_3}\{\hat{\mathbf{Q}}_A^t\mathbf{N}\hat{\mathbf{Q}}_B\}\mathrm{d}^2\mathbf{x}_H = \int_{\mathbb{R}^2} \hat{\mathbf{Q}}_A^t(\hat{\boldsymbol{\mathcal{A}}}^t\mathbf{N} + \mathbf{N}\hat{\boldsymbol{\mathcal{A}}})\hat{\mathbf{Q}}_B\mathrm{d}^2\mathbf{x}_H. \tag{A6}$$

From equation (A3) it follows that the right-hand side is equal to zero. Integrating the left-hand side over x_3 from $x_{3,1}$ to $x_{3,m}$ (which are the depth levels of boundaries $\partial\mathrm{D}_1$ and $\partial\mathrm{D}_m$) we obtain

$$\int_{\partial\mathrm{D}_1} \hat{\mathbf{Q}}_A^t\mathbf{N}\hat{\mathbf{Q}}_B\,\mathrm{d}^2\mathbf{x} = \int_{\partial\mathrm{D}_m} \hat{\mathbf{Q}}_A^t\mathbf{N}\hat{\mathbf{Q}}_B\,\mathrm{d}^2\mathbf{x}. \tag{A7}$$

At the boundaries $\partial\mathrm{D}_1$ and $\partial\mathrm{D}_m$ we decompose operator matrix $\hat{\boldsymbol{\mathcal{A}}}$ as follows

$$\hat{\boldsymbol{\mathcal{A}}} = \hat{\boldsymbol{\mathcal{L}}}\hat{\boldsymbol{\mathcal{H}}}\hat{\boldsymbol{\mathcal{L}}}^{-1} \tag{A8}$$

(Corones *et al.* 1983, 1992; Fishman *et al.* 1987; de Hoop 1992, 1996; Fishman 1993; Haines and de Hoop 1996; Wapenaar *et al.* 2001). Examples of this decomposition are given in Appendices B and C. We scale the operator $\hat{\boldsymbol{\mathcal{L}}}$ in such a way that

$$\hat{\boldsymbol{\mathcal{L}}}^t\mathbf{N}\hat{\boldsymbol{\mathcal{L}}} = -\mathbf{N} \quad \text{or} \quad \hat{\boldsymbol{\mathcal{L}}}^{-1} = -\mathbf{N}^{-1}\hat{\boldsymbol{\mathcal{L}}}^t\mathbf{N} \tag{A9}$$

(de Hoop 1992; Wapenaar, Dillen and Fokkema 2001). Using this specific scaling, we introduce the $K \times 1$ flux-normalized decomposed field vector $\hat{\mathbf{P}} = \hat{\mathbf{P}}(\mathbf{x}, \omega)$ via

$$\hat{\mathbf{Q}} = \hat{\boldsymbol{\mathcal{L}}}\hat{\mathbf{P}} \quad \text{and} \quad \hat{\mathbf{P}} = \hat{\boldsymbol{\mathcal{L}}}^{-1}\hat{\mathbf{Q}}, \tag{A10}$$

with

$$\hat{\mathbf{P}} = \begin{pmatrix} \hat{\mathbf{P}}^+ \\ \hat{\mathbf{P}}^- \end{pmatrix}, \tag{A11}$$

where $\frac{K}{2} \times 1$ vectors $\hat{\mathbf{P}}^+ = \hat{\mathbf{P}}^+(\mathbf{x}, \omega)$ and $\hat{\mathbf{P}}^- = \hat{\mathbf{P}}^-(\mathbf{x}, \omega)$ represent down going and up going fields, respectively (for scalar fields we have $\hat{\mathbf{P}}^+ = \hat{p}^+$ and $\hat{\mathbf{P}}^- = \hat{p}^-$). Here 'down going' and 'up going' should be interpreted in a broad sense: for diffusion fields these terms mean 'decaying in the positive or negative x_3-direction, respectively'. Substitution of $\hat{\mathbf{Q}} = \hat{\boldsymbol{\mathcal{L}}}\hat{\mathbf{P}}$ into equation (A7) gives, using equation (A2),

$$\int_{\partial\mathrm{D}_1} \hat{\mathbf{P}}_A^t\hat{\boldsymbol{\mathcal{L}}}^t\mathbf{N}\hat{\boldsymbol{\mathcal{L}}}\hat{\mathbf{P}}_B\,\mathrm{d}^2\mathbf{x} = \int_{\partial\mathrm{D}_m} \hat{\mathbf{P}}_A^t\hat{\boldsymbol{\mathcal{L}}}^t\mathbf{N}\hat{\boldsymbol{\mathcal{L}}}\hat{\mathbf{P}}_B\,\mathrm{d}^2\mathbf{x}, \tag{A12}$$

or, using $\hat{\boldsymbol{\mathcal{L}}}^t\mathbf{N}\hat{\boldsymbol{\mathcal{L}}} = -\mathbf{N}$,

$$\int_{\partial\mathrm{D}_1} \hat{\mathbf{P}}_A^t\mathbf{N}\hat{\mathbf{P}}_B\,\mathrm{d}^2\mathbf{x} = \int_{\partial\mathrm{D}_m} \hat{\mathbf{P}}_A^t\mathbf{N}\hat{\mathbf{P}}_B\,\mathrm{d}^2\mathbf{x}. \tag{A13}$$

Substitution of equations (A4) and (A11) into equation (A13) yields equation (2) (for $K = 2$) or equation (16) (for all other cases).

APPENDIX B: DECOMPOSITION OPERATORS FOR SCALAR FIELDS

We discuss the field vectors and operators introduced in Appendix A for scalar fields ($K = 2$). For an acoustic wave field in a dissipative 3D inhomogeneous fluid we have (de Hoop 1992; Wapenaar *et al.* 2001)

$$\hat{\mathbf{Q}} = \begin{pmatrix} \hat{p} \\ \hat{v}_3 \end{pmatrix}, \quad \hat{\boldsymbol{\mathcal{A}}} = \begin{pmatrix} 0 & -j\omega\hat{\rho} \\ \frac{1}{j\omega\hat{\rho}^{\frac{1}{2}}}(\hat{\mathcal{H}}_2\hat{\rho}^{-\frac{1}{2}}\cdot) & 0 \end{pmatrix}, \tag{B1}$$

where $\hat{p} = \hat{p}(\mathbf{x}, \omega)$ is the acoustic pressure, $\hat{v}_3 = \hat{v}_3(\mathbf{x}, \omega)$ the vertical component of the particle velocity and $\hat{\rho} = \hat{\rho}(\mathbf{x}, \omega)$ the complex-valued mass density of the dissipative medium. $\hat{\mathcal{H}}_2$ is the Helmholtz operator, defined as

$$\hat{\mathcal{H}}_2 = \frac{\omega^2}{\hat{c}^2} + \frac{\partial}{\partial x_\alpha}\frac{\partial}{\partial x_\alpha}. \tag{B2}$$

The summation convention applies for repeated subscripts; Greek subscripts take on the values 1 and 2. In equation (B2), $\hat{c} = \hat{c}(\mathbf{x}, \omega)$ is the complex-valued propagation velocity, obeying the Klein-Gordon dispersion relation known from relativistic quantum mechanics (Messiah 1962; Anno, Cohen and Bleistein 1992), according to

$$\frac{\omega^2}{\hat{c}^2} = \omega^2\hat{\kappa}\hat{\rho} - \frac{3}{4\hat{\rho}^2}\frac{\partial\hat{\rho}}{\partial x_\alpha}\frac{\partial\hat{\rho}}{\partial x_\alpha} + \frac{1}{2\hat{\rho}}\frac{\partial}{\partial x_\alpha}\frac{\partial\hat{\rho}}{\partial x_\alpha}, \tag{B3}$$

with $\hat{\kappa} = \hat{\kappa}(\mathbf{x}, \omega)$ the complex-valued compressibility of the dissipative medium. Note that $\hat{\mathcal{H}}_2 = \hat{\mathcal{H}}_2^t$, hence, symmetry relation (A3) is fulfilled. The decomposition of $\hat{\boldsymbol{\mathcal{A}}}$ is given by

Table B1 Overview of field quantities and medium parameters in equations (B1)–(B7).

	field quantities in $\hat{\mathbf{Q}}$		medium parameters in $\hat{\boldsymbol{\mathcal{A}}}$, $\hat{\boldsymbol{\mathcal{H}}}$, $\hat{\boldsymbol{\mathcal{L}}}$ and $\hat{\boldsymbol{\mathcal{L}}}^{-1}$	
3D Acoustic	$\hat{p}$	$\hat{v}_3$	$\hat{\kappa}$	$\hat{\rho}$
3D Diffusion	$\hat{Y}$	$\hat{J}_3$	ρ	$1/j\omega\rho\mathcal{D}$
2D SH	$\hat{v}_2$	$-\hat{\tau}_{23}$	$\hat{\rho}$	$1/\hat{\mu}$
2D TE	$\hat{E}_2$	$-\hat{H}_1$	$\hat{\varepsilon}+\hat{\sigma}/j\omega$	$\hat{\mu}+\hat{\Gamma}/j\omega$
2D TM	$\hat{H}_2$	$\hat{E}_1$	$\hat{\mu}+\hat{\Gamma}/j\omega$	$\hat{\varepsilon}+\hat{\sigma}/j\omega$

equation (A8), where

$$\hat{\boldsymbol{\mathcal{H}}}=\begin{pmatrix}-j\hat{\mathcal{H}}_1 & 0\\ 0 & j\hat{\mathcal{H}}_1\end{pmatrix},\quad \hat{\mathcal{H}}_1=\hat{\mathcal{H}}_2^{\frac{1}{2}}, \tag{B4}$$

with $\hat{\mathcal{H}}_1=\hat{\mathcal{H}}_1^t$ (Wapenaar, Dillen and Fokkema 2001), and

$$\hat{\boldsymbol{\mathcal{L}}}=\begin{pmatrix}\hat{\mathcal{L}}_1 & \hat{\mathcal{L}}_1\\ \hat{\mathcal{L}}_2 & -\hat{\mathcal{L}}_2\end{pmatrix},\ \hat{\boldsymbol{\mathcal{L}}}^{-1}=\frac{1}{2}\begin{pmatrix}\hat{\mathcal{L}}_1^{-1} & \hat{\mathcal{L}}_2^{-1}\\ \hat{\mathcal{L}}_1^{-1} & -\hat{\mathcal{L}}_2^{-1}\end{pmatrix}, \tag{B5}$$

with

$$\hat{\mathcal{L}}_1=\left(\frac{\omega\hat{\rho}}{2}\right)^{\frac{1}{2}}\hat{\mathcal{H}}_1^{-\frac{1}{2}},\quad \frac{1}{2}\hat{\mathcal{L}}_1^{-1}=\hat{\mathcal{L}}_2^t=\hat{\mathcal{H}}_1^{\frac{1}{2}}\left(\frac{1}{2\omega\hat{\rho}}\right)^{\frac{1}{2}}, \tag{B6}$$

$$\hat{\mathcal{L}}_2=\left(\frac{1}{2\omega\hat{\rho}}\right)^{\frac{1}{2}}\hat{\mathcal{H}}_1^{\frac{1}{2}},\quad \frac{1}{2}\hat{\mathcal{L}}_2^{-1}=\hat{\mathcal{L}}_1^t=\hat{\mathcal{H}}_1^{-\frac{1}{2}}\left(\frac{\omega\hat{\rho}}{2}\right)^{\frac{1}{2}}, \tag{B7}$$

with $\hat{\mathcal{H}}_1^{\frac{1}{2}}=(\hat{\mathcal{H}}_1^{\frac{1}{2}})^t$ and $\hat{\mathcal{H}}_1^{-\frac{1}{2}}=(\hat{\mathcal{H}}_1^{-\frac{1}{2}})^t$. Note that symmetry relation (A9) is fulfilled as well.The field quantities and medium parameters involved in acoustic decomposition are summarized in the first row of Table B1. In a dissipative fluid the imaginary parts of $\hat{\rho}$ and $\hat{\kappa}$ are negative (for positive ω). The imaginary part of the eigenvalue spectrum of the square-root operator $\hat{\mathcal{H}}_1$ is chosen negative as well (Wapenaar *et al.* 2001). The same applies for the spectrum of $\hat{\mathcal{H}}_1^{\frac{1}{2}}$, i.e., the square-root of the square-root operator. For mass diffusion of a species through a mixture, $\hat{\mathbf{Q}}$ is given by

$$\hat{\mathbf{Q}}=\begin{pmatrix}\hat{Y}\\ \hat{J}_3\end{pmatrix}, \tag{B8}$$

where $\hat{Y}=\hat{Y}(\mathbf{x},\omega)$ is the mass fraction of the species and $\hat{J}_3=\hat{J}_3(\mathbf{x},\omega)$ the vertical component of the mass flux relative to the mixture. In equations (B1)–(B7) we replace the quantities in the first row of Table B1 by those in the second row (where $\mathcal{D}$ is the diffusion coefficient). We thus obtain the decomposition operators for mass diffusion. Note that the term $1/j\omega\rho\mathcal{D}$ is purely negative imaginary (for positive ω). The imaginary parts of the spectra of $\hat{\mathcal{H}}_1$ and $\hat{\mathcal{H}}_1^{\frac{1}{2}}$ are again chosen as negative as well.

The last three rows in Table B1 show the field quantities and medium parameters for three other applications of equations (B1)–(B7), but this time for the 2D situation (i.e. assuming that the field quantities and medium parameters are independent of the x_2-coordinate). 'SH' stands for horizontally polarized shear waves. In this row $\hat{\tau}_{23}$ is the shear stress and $\hat{\mu}$ the shear modulus of the medium. 'TE' and 'TM' stand for transverse electric and transverse magnetic fields, respectively. $\hat{E}_{1,2}$ and $\hat{H}_{1,2}$ are the electric and magnetic field components, $\hat{\varepsilon}$ is the permittivity, $\hat{\mu}$ the permeability, $\hat{\sigma}$ the conductivity and $\hat{\Gamma}$ the magnetic hysteresis loss term. Note that depending on the choices of the medium parameters, the TE and TM fields can be wave or diffusion fields, or a combination of the two. In all cases the imaginary parts of the spectra of $\hat{\mathcal{H}}_1$ and $\hat{\mathcal{H}}_1^{\frac{1}{2}}$ are chosen negative.

APPENDIX C: DECOMPOSITION OPERATORS FOR VECTOR FIELDS

For 3D electromagnetic diffusion and/or wave propagation in a dissipative 3D inhomogeneous medium we have (Reid 1972)

$$\hat{\mathbf{Q}}=\begin{pmatrix}\hat{E}_1\\ \hat{E}_2\\ \hat{H}_2\\ -\hat{H}_1\end{pmatrix},\quad \hat{\boldsymbol{\mathcal{A}}}=\begin{pmatrix}\mathbf{O} & \hat{\boldsymbol{\mathcal{A}}}_{12}\\ \hat{\boldsymbol{\mathcal{A}}}_{21} & \mathbf{O}\end{pmatrix}, \tag{C1}$$

where

$$\hat{\boldsymbol{\mathcal{A}}}_{12}=\begin{pmatrix}-j\omega\hat{\mathcal{M}}+\frac{1}{j\omega}\frac{\partial}{\partial x_1}\left(\frac{1}{\hat{\mathcal{E}}}\frac{\partial}{\partial x_1}\cdot\right) & \frac{1}{j\omega}\frac{\partial}{\partial x_1}\left(\frac{1}{\hat{\mathcal{E}}}\frac{\partial}{\partial x_2}\cdot\right)\\ \frac{1}{j\omega}\frac{\partial}{\partial x_2}\left(\frac{1}{\hat{\mathcal{E}}}\frac{\partial}{\partial x_1}\cdot\right) & -j\omega\hat{\mathcal{M}}+\frac{1}{j\omega}\frac{\partial}{\partial x_2}\left(\frac{1}{\hat{\mathcal{E}}}\frac{\partial}{\partial x_2}\cdot\right)\end{pmatrix}, \tag{C2}$$

$$\hat{\boldsymbol{\mathcal{A}}}_{21}=\begin{pmatrix}-j\omega\hat{\mathcal{E}}+\frac{1}{j\omega}\frac{\partial}{\partial x_2}\left(\frac{1}{\hat{\mathcal{M}}}\frac{\partial}{\partial x_2}\cdot\right) & -\frac{1}{j\omega}\frac{\partial}{\partial x_2}\left(\frac{1}{\hat{\mathcal{M}}}\frac{\partial}{\partial x_1}\cdot\right)\\ -\frac{1}{j\omega}\frac{\partial}{\partial x_1}\left(\frac{1}{\hat{\mathcal{M}}}\frac{\partial}{\partial x_2}\cdot\right) & -j\omega\hat{\mathcal{E}}+\frac{1}{j\omega}\frac{\partial}{\partial x_1}\left(\frac{1}{\hat{\mathcal{M}}}\frac{\partial}{\partial x_1}\cdot\right)\end{pmatrix}, \tag{C3}$$

with

$$\hat{\mathcal{E}}=\hat{\varepsilon}+\hat{\sigma}/j\omega,\quad \hat{\mathcal{M}}=\hat{\mu}+\hat{\Gamma}/j\omega. \tag{C4}$$

Note that $\hat{\boldsymbol{\mathcal{A}}}$ obeys symmetry relation (A3) in an arbitrary 3D inhomogeneous dissipative medium, which validates

reciprocity theorem (A7). Next, for the decomposition of $\hat{\boldsymbol{\mathcal{A}}}$ at $\partial\mathrm{D}_1$ and $\partial\mathrm{D}_m$ we assume that there are no lateral variations of the medium parameters at these boundaries. We define the two-dimensional spatial Fourier transform from the space-frequency domain to the wavenumber-frequency domain as follows

$$\tilde{f}(\mathbf{k}_H, x_3, \omega) = \int_{\mathbb{R}^2} \hat{f}(\mathbf{x}_H, x_3, \omega) \exp\{j\mathbf{k}_H \cdot \mathbf{x}_H\} \mathrm{d}^2\mathbf{x}_H, \tag{C5}$$

with $\mathbf{k}_H = (k_1, k_2)$. Applying this transform to equation (A8) gives

$$\tilde{\boldsymbol{\mathcal{A}}} = \tilde{\boldsymbol{\mathcal{L}}}\tilde{\boldsymbol{\mathcal{H}}}\tilde{\boldsymbol{\mathcal{L}}}^{-1}, \tag{C6}$$

where $\tilde{\boldsymbol{\mathcal{A}}}$ is obtained from $\hat{\boldsymbol{\mathcal{A}}}$ defined in equations (C1)–(C3) by replacing $\partial/\partial\, x_\alpha$ by $-jk_\alpha$. Note that equation (A3) transforms to

$$\tilde{\boldsymbol{\mathcal{A}}}^t(-\mathbf{k}_H, x_3, \omega)\mathbf{N} = -\mathbf{N}\tilde{\boldsymbol{\mathcal{A}}}(\mathbf{k}_H, x_3, \omega). \tag{C7}$$

The sign-change of $\mathbf{k}_H$ in the argument of the transposed matrix is due to the relation $(\partial/\partial x_\alpha)^t = -\partial/\partial x_\alpha$. Similarly, equation (C9) transforms to

$$\{\tilde{\boldsymbol{\mathcal{L}}}(-\mathbf{k}_H, x_3, \omega)\}^t\mathbf{N}\tilde{\boldsymbol{\mathcal{L}}}(\mathbf{k}_H, x_3, \omega) = -\mathbf{N}, \tag{C8}$$

or

$$\{\tilde{\boldsymbol{\mathcal{L}}}(\mathbf{k}_H, x_3, \omega)\}^{-1} = -\mathbf{N}^{-1}\{\tilde{\boldsymbol{\mathcal{L}}}(-\mathbf{k}_H, x_3, \omega)\}^t\mathbf{N}. \tag{C9}$$

With this scaling we obtain (Ursin 1983)

$$\tilde{\boldsymbol{\mathcal{H}}} = \begin{pmatrix} -j\tilde{\boldsymbol{\mathcal{H}}}_1 & \mathrm{O} \\ \mathrm{O} & j\tilde{\boldsymbol{\mathcal{H}}}_1 \end{pmatrix}, \quad \tilde{\boldsymbol{\mathcal{H}}}_1 = \begin{pmatrix} \tilde{\mathcal{H}}_1 & 0 \\ 0 & \tilde{\mathcal{H}}_1 \end{pmatrix}, \tag{C10}$$

$$\tilde{\boldsymbol{\mathcal{L}}} = \begin{pmatrix} \tilde{\boldsymbol{\mathcal{L}}}_1 & \tilde{\boldsymbol{\mathcal{L}}}_1 \\ \tilde{\boldsymbol{\mathcal{L}}}_2 & -\tilde{\boldsymbol{\mathcal{L}}}_2 \end{pmatrix}, \tilde{\boldsymbol{\mathcal{L}}}^{-1} = \frac{1}{2}\begin{pmatrix} \tilde{\boldsymbol{\mathcal{L}}}_1^{-1} & \tilde{\boldsymbol{\mathcal{L}}}_2^{-1} \\ \tilde{\boldsymbol{\mathcal{L}}}_1^{-1} & -\tilde{\boldsymbol{\mathcal{L}}}_2^{-1} \end{pmatrix}, \tag{C11}$$

where

$$\tilde{\boldsymbol{\mathcal{L}}}_1(\mathbf{k}_H, x_3, \omega) = \frac{1}{\sqrt{2}}\begin{pmatrix} \hat{\zeta}\tilde{\mathcal{H}}_1^{-1/2} & 0 \\ -\frac{k_1k_2}{\omega\hat{\mathcal{E}}\hat{\zeta}}\tilde{\mathcal{H}}_1^{-1/2} & \hat{\vartheta}^{-1}\tilde{\mathcal{H}}_1^{1/2} \end{pmatrix}, \tag{C12}$$

$$\tilde{\boldsymbol{\mathcal{L}}}_2(\mathbf{k}_H, x_3, \omega) = \frac{1}{\sqrt{2}}\begin{pmatrix} \hat{\zeta}^{-1}\tilde{\mathcal{H}}_1^{1/2} & \frac{k_1k_2}{\omega\hat{\mathcal{M}}\hat{\vartheta}}\tilde{\mathcal{H}}_1^{-1/2} \\ 0 & \hat{\vartheta}\tilde{\mathcal{H}}_1^{-1/2} \end{pmatrix}, \tag{C13}$$

$$\frac{1}{2}\{\tilde{\boldsymbol{\mathcal{L}}}_1(\mathbf{k}_H, x_3, \omega)\}^{-1} = \{\tilde{\boldsymbol{\mathcal{L}}}_2(-\mathbf{k}_H, x_3, \omega)\}^t, \tag{C14}$$

$$\frac{1}{2}\{\tilde{\boldsymbol{\mathcal{L}}}_2(\mathbf{k}_H, x_3, \omega)\}^{-1} = \{\tilde{\boldsymbol{\mathcal{L}}}_1(-\mathbf{k}_H, x_3, \omega)\}^t, \tag{C15}$$

with

$$\tilde{\mathcal{H}}_1 = \sqrt{k^2 - k_\alpha k_\alpha}, \quad \Im(\tilde{\mathcal{H}}_1) < 0, \tag{C16}$$

$$k^2 = \frac{\omega^2}{\hat{c}^2} = \omega^2\hat{\mathcal{E}}\hat{\mathcal{M}}, \tag{C17}$$

$$\hat{\zeta} = \left(\omega\hat{\mathcal{M}} - \frac{k_1^2}{\omega\hat{\mathcal{E}}}\right)^{1/2}, \quad \hat{\vartheta} = \left(\omega\hat{\mathcal{E}} - \frac{k_1^2}{\omega\hat{\mathcal{M}}}\right)^{1/2}. \tag{C18}$$

For an elastodynamic wave field in a dissipative inhomogeneous anisotropic solid we have (Woodhouse 1974)

$$\hat{\mathbf{Q}} = \begin{pmatrix} -\hat{\boldsymbol{\tau}}_3 \\ \hat{\mathbf{v}} \end{pmatrix}, \quad \hat{\boldsymbol{\mathcal{A}}} = \begin{pmatrix} \hat{\boldsymbol{\mathcal{A}}}_{11} & \hat{\boldsymbol{\mathcal{A}}}_{12} \\ \hat{\boldsymbol{\mathcal{A}}}_{21} & \hat{\boldsymbol{\mathcal{A}}}_{22} \end{pmatrix}, \tag{C19}$$

where $\hat{\boldsymbol{\tau}}_3 = \hat{\boldsymbol{\tau}}_3(\mathbf{x}, \omega)$ is the traction vector and $\hat{\mathbf{v}} = \hat{\mathbf{v}}(\mathbf{x}, \omega)$ the particle velocity vector,

$$\hat{\boldsymbol{\mathcal{A}}}_{11} = -\frac{\partial}{\partial x_\alpha}\left(\hat{\mathbf{C}}_{\alpha 3}\hat{\mathbf{C}}_{33}^{-1}\,\cdot\right), \tag{C20}$$

$$\hat{\boldsymbol{\mathcal{A}}}_{12} = -j\omega\hat{\rho}\mathbf{I} + \frac{1}{j\omega}\frac{\partial}{\partial x_\alpha}\left(\hat{\mathbf{U}}_{\alpha\beta}\frac{\partial}{\partial x_\beta}\,\cdot\right), \tag{C21}$$

$$\hat{\boldsymbol{\mathcal{A}}}_{21} = -j\omega\hat{\mathbf{C}}_{33}^{-1}, \tag{C22}$$

$$\hat{\boldsymbol{\mathcal{A}}}_{22} = -\hat{\mathbf{C}}_{33}^{-1}\hat{\mathbf{C}}_{3\beta}\frac{\partial}{\partial x_\beta}, \tag{C23}$$

$$\hat{\mathbf{U}}_{\alpha\beta} = \hat{\mathbf{C}}_{\alpha\beta} - \hat{\mathbf{C}}_{\alpha 3}\hat{\mathbf{C}}_{33}^{-1}\hat{\mathbf{C}}_{3\beta}, \tag{C24}$$

with $(\hat{\mathbf{C}}_{jl})_{ik} = \hat{c}_{ijkl}$. Here $\hat{c}_{ijkl} = \hat{c}_{ijkl}(\mathbf{x}, \omega)$ is the complex-valued stiffness tensor and $\hat{\rho} = \hat{\rho}(\mathbf{x}, \omega)$ the complex-valued mass density of the dissipative medium. Since $\hat{c}_{ijkl} = \hat{c}_{klij}$, $\hat{\boldsymbol{\mathcal{A}}}$ obeys symmetry relation (A3) in an arbitrary 3D inhomogeneous anisotropic dissipative medium. This validates reciprocity theorem (A7). Next, for the decomposition of $\hat{\boldsymbol{\mathcal{A}}}$ at $\partial\mathrm{D}_1$ and $\partial\mathrm{D}_m$ we assume that the medium is laterally invariant and isotropic at these boundaries, hence

$$(\hat{\mathbf{C}}_{jl})_{ik} = \hat{c}_{ijkl} = \hat{\lambda}\delta_{ij}\delta_{kl} + \hat{\mu}(\delta_{ik}\delta_{jl} + \delta_{il}\delta_{jk}), \tag{C25}$$

where $\hat{\lambda}$ and $\hat{\mu}$ are the complex-valued Lamé parameters at $\partial\mathrm{D}_1$ and $\partial\mathrm{D}_m$. The decomposition of $\hat{\boldsymbol{\mathcal{A}}}$ is again defined by equation (C6) in the wavenumber-frequency domain. By scaling the matrices such that equations (C8) and (C9) are obeyed, we find [modified after Frasier (1970); Ursin (1983)]

$$\tilde{\boldsymbol{\mathcal{H}}} = \begin{pmatrix} -j\tilde{\boldsymbol{\mathcal{H}}}_1 & \mathrm{O} \\ \mathrm{O} & j\tilde{\boldsymbol{\mathcal{H}}}_1 \end{pmatrix}, \quad \tilde{\boldsymbol{\mathcal{H}}}_1 = \begin{pmatrix} \tilde{\mathcal{H}}_{1,P} & 0 & 0 \\ 0 & \tilde{\mathcal{H}}_{1,S} & 0 \\ 0 & 0 & \tilde{\mathcal{H}}_{1,S} \end{pmatrix}, \tag{C26}$$

$$\tilde{\boldsymbol{\mathcal{L}}} = \begin{pmatrix} \tilde{\boldsymbol{\mathcal{L}}}_1^+ & \tilde{\boldsymbol{\mathcal{L}}}_1^- \\ \tilde{\boldsymbol{\mathcal{L}}}_2^+ & \tilde{\boldsymbol{\mathcal{L}}}_2^- \end{pmatrix}, \tilde{\boldsymbol{\mathcal{L}}}^{-1} = \begin{pmatrix} \tilde{\boldsymbol{\mathcal{N}}}_1^+ & \tilde{\boldsymbol{\mathcal{N}}}_2^+ \\ \tilde{\boldsymbol{\mathcal{N}}}_1^- & \tilde{\boldsymbol{\mathcal{N}}}_2^- \end{pmatrix}, \tag{C27}$$

where

$$\tilde{\boldsymbol{\mathcal{L}}}_1^{\pm}(\mathbf{k}_H, x_3, \omega) = \frac{\hat{\mu}}{\omega^{3/2}(2\hat{\rho})^{1/2}} \begin{pmatrix} \pm 2k_1\tilde{\mathcal{H}}_{1,P}^{1/2} & \mp\frac{k_1(k_S^2-2k_r^2)}{k_r\tilde{\mathcal{H}}_{1,S}^{1/2}} & \mp\frac{k_2 k_S\tilde{\mathcal{H}}_{1,S}^{1/2}}{k_r} \\ \pm 2k_2\tilde{\mathcal{H}}_{1,P}^{1/2} & \mp\frac{k_2(k_S^2-2k_r^2)}{k_r\tilde{\mathcal{H}}_{1,S}^{1/2}} & \pm\frac{k_1 k_S\tilde{\mathcal{H}}_{1,S}^{1/2}}{k_r} \\ \frac{(k_S^2-2k_r^2)}{\tilde{\mathcal{H}}_{1,P}^{1/2}} & 2k_r\tilde{\mathcal{H}}_{1,S}^{1/2} & 0 \end{pmatrix}, \tag{C28}$$

$$\tilde{\boldsymbol{\mathcal{L}}}_2^{\pm}(\mathbf{k}_H, x_3, \omega) = \frac{1}{\omega^{1/2}(2\hat{\rho})^{1/2}} \begin{pmatrix} \frac{k_1}{\tilde{\mathcal{H}}_{1,P}^{1/2}} & -\frac{k_1\tilde{\mathcal{H}}_{1,S}^{1/2}}{k_r} & -\frac{k_2 k_S}{k_r\tilde{\mathcal{H}}_{1,S}^{1/2}} \\ \frac{k_2}{\tilde{\mathcal{H}}_{1,P}^{1/2}} & -\frac{k_2\tilde{\mathcal{H}}_{1,S}^{1/2}}{k_r} & \frac{k_1 k_S}{k_r\tilde{\mathcal{H}}_{1,S}^{1/2}} \\ \pm\tilde{\mathcal{H}}_{1,P}^{1/2} & \pm\frac{k_r}{\tilde{\mathcal{H}}_{1,S}^{1/2}} & 0 \end{pmatrix}, \tag{C29}$$

$$\tilde{\boldsymbol{\mathcal{N}}}_1^{\pm}(\mathbf{k}_H, x_3, \omega) = \mp\{\tilde{\boldsymbol{\mathcal{L}}}_2^{\mp}(-\mathbf{k}_H, x_3, \omega)\}^t, \tag{C30}$$

$$\tilde{\boldsymbol{\mathcal{N}}}_2^{\pm}(\mathbf{k}_H, x_3, \omega) = \pm\{\tilde{\boldsymbol{\mathcal{L}}}_1^{\mp}(-\mathbf{k}_H, x_3, \omega)\}^t, \tag{C31}$$

with

$$\tilde{\mathcal{H}}_{1,P} = \sqrt{k_P^2 - k_\alpha k_\alpha}, \quad \Im(\tilde{\mathcal{H}}_{1,P}) < 0, \tag{C32}$$

$$\tilde{\mathcal{H}}_{1,S} = \sqrt{k_S^2 - k_\alpha k_\alpha}, \quad \Im(\tilde{\mathcal{H}}_{1,S}) < 0, \tag{C33}$$

$$k_P^2 = \frac{\omega^2}{\hat{c}_P^2} = \frac{\hat{\rho}\omega^2}{\hat{\lambda}+2\hat{\mu}}, \tag{C34}$$

$$k_S^2 = \frac{\omega^2}{\hat{c}_S^2} = \frac{\hat{\rho}\omega^2}{\hat{\mu}}, \tag{C35}$$

$$k_r = \sqrt{k_1^2 + k_2^2}. \tag{C36}$$

For the 2D situation (i.e. assuming that the field quantities and medium parameters are independent of the x_2-coordinate), the elastodynamic wave field decouples into horizontally polarized shear waves (*SH*-waves) and waves polarized in the vertical plane (*P* and *SV* waves). The matrices for *SH*-waves were discussed in Appendix A. The matrices for *P* and *SV* waves can be obtained from equations (C28) and (C29) by setting k_2 to zero and deleting all matrix elements that are equal to zero. The disadvantage of this approach is that the resulting matrices will contain terms proportional to the discontinuous functions $k_r = |k_1|$ and $k_1/|k_1| = \text{sign}\,(k_1)$. As an alternative, we may define $\tilde{\boldsymbol{\mathcal{L}}}_1^{\pm}(k_1, x_3, \omega)$ and $\tilde{\boldsymbol{\mathcal{L}}}_2^{\pm}(k_1, x_3, \omega)$ as follows

$$\tilde{\boldsymbol{\mathcal{L}}}_1^{\pm}(k_1, x_3, \omega) = \frac{\hat{\mu}}{\omega^{3/2}(2\hat{\rho})^{1/2}} \begin{pmatrix} \pm 2k_1\tilde{\mathcal{H}}_{1,P}^{1/2} & -\frac{(k_S^2-2k_1^2)}{\tilde{\mathcal{H}}_{1,S}^{1/2}} \\ \frac{(k_S^2-2k_1^2)}{\tilde{\mathcal{H}}_{1,P}^{1/2}} & \pm 2k_1\tilde{\mathcal{H}}_{1,S}^{1/2} \end{pmatrix}, \tag{C37}$$

$$\tilde{\boldsymbol{\mathcal{L}}}_2^{\pm}(k_1, x_3, \omega) = \frac{1}{\omega^{1/2}(2\hat{\rho})^{1/2}} \begin{pmatrix} \frac{k_1}{\tilde{\mathcal{H}}_{1,P}^{1/2}} & \mp\tilde{\mathcal{H}}_{1,S}^{1/2} \\ \pm\tilde{\mathcal{H}}_{1,P}^{1/2} & \frac{k_1}{\tilde{\mathcal{H}}_{1,S}^{1/2}} \end{pmatrix}. \tag{C38}$$

With these choices the above mentioned discontinuities are avoided and equations (C8) and (C9) are again obeyed.With the matrices discussed in this appendix, wave field decomposition at $\partial\mathrm{D}_1$ and $\partial\mathrm{D}_m$ is accomplished through

$$\tilde{\mathbf{P}} = \tilde{\boldsymbol{\mathcal{L}}}^{-1}\tilde{\mathbf{Q}}, \tag{C39}$$

or, applying an inverse spatial Fourier transform,

$$\hat{\mathbf{P}}(\mathbf{x}, \omega) = \left(\frac{1}{2\pi}\right)^2 \int_{\mathbb{R}^2} \tilde{\boldsymbol{\mathcal{L}}}^{-1}\tilde{\mathbf{Q}} \exp\{-j\mathbf{k}_H \cdot \mathbf{x}_H\} \mathrm{d}^2\mathbf{k}_H. \tag{C40}$$

This decomposition is exact when the medium parameters at $\partial\mathrm{D}_1$ and $\partial\mathrm{D}_m$ are laterally invariant (everywhere else the medium can be arbitrarily inhomogeneous). When the medium parameters at $\partial\mathrm{D}_1$ and $\partial\mathrm{D}_m$ are smoothly varying, this equation can still be used in an approximate sense. To this end $\tilde{\boldsymbol{\mathcal{L}}}^{-1}(\mathbf{k}_H, x_3, \omega)$ should be replaced by $\tilde{\boldsymbol{\mathcal{L}}}^{-1}(\mathbf{k}_H, \mathbf{x}, \omega)$, based on the local medium parameters at $\mathbf{x}$ on $\partial\mathrm{D}_1$ and $\partial\mathrm{D}_m$.